# Supporting Information

## Naphthalene-imide Self-Assembled Monolayers as a Surface Modification of ITO for Improved Thermal Stability of Perovskite Solar Cells

Sebastian O. Fürer,[1,2,3*] Kevin J. Rietwyk,[1,2] Federico Pulvirenti,[3] David P. McMeekin,[1,2] Maciej Adam Surmiak,[1,2] Sonia R. Raga,[1,2,4] Wenxin Mao,[1,2] Xiongfeng Lin,[1,2] Yvonne Hora,[1,2] Jian Wang,[5] Yangwei Shi,[5,6] Stephen Barlow,[3,7] David S. Ginger,[5] Seth R. Marder,[3,7,8*] Udo Bach[1,2*]

[1] *Department of Chemical and Biological Engineering, Monash University, Clayton, Victoria 3800, Australia*
[2] *ARC Centre of Excellence in Exciton Science, Monash University, Clayton, Victoria 3800, Australia*
[3] *School of Chemistry and Biochemistry, Georgia Institute of Technology, Atlanta, Georgia 30332, USA*
[4] *Institut Català de Nanociència i Nanotecnologia, Universitat Autònoma de Barcelona, 08193 Bellaterra, Barcelona, Spain*
[5] *Department of Chemistry, University of Washington, Seattle, Washington 98195, USA*
[6] *Molecular Engineering and Sciences Institute, University of Washington, Seattle, Washington 98195, USA*
[7] *Renewable and Sustainable Energy Institute, University of Colorado Boulder, Boulder, Colorado 80303, USA*
[8] *Departments of Chemical and Biological Engineering and of Chemistry, University of Colorado Boulder, Boulder, Colorado 80303, USA*

[*] Corresponding author email: sebastian.furer@monash.edu, udo.bach@monash.edu, seth.marder@colorado.edu

# Table of Contents

## 1. Thermal Properties

DSC and TGA experiments were performed on Mettler-Toledo TA instruments in air at a scan rate of 10 °C $min^{-1}$. $T_d$ is defined based on 5% weight loss.

**Table S1.** Thermal Properties of NMIs **2a-d** and NDIs **3a-d** determined by TGA measurements in air with a scan rate of 10 °C $min^{-1}$.

| | $T_d$, °C |
|---|---|
| **2a** | 177 |
| **2b** | 219 |
| **2c** | 186 |
| **2d** | 202 |
| **3a** | 365 |
| **3b** | 308 |
| **3c** | 324 |
| **3d** | 223 |

## 2. Cyclic Voltammetry

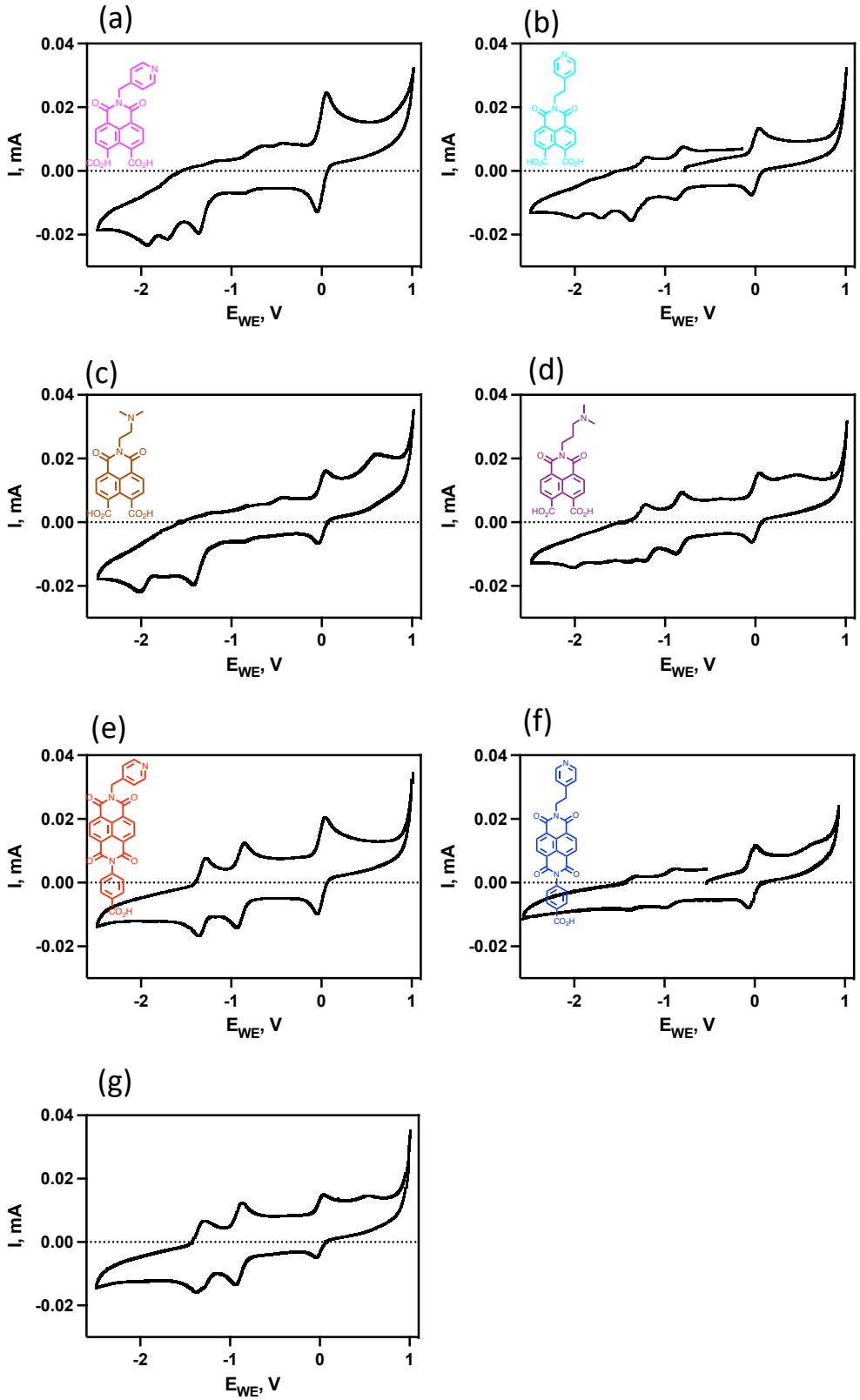


**Figure S1.** Cyclic voltammograms (CVs) of a) **2a**, b) **2b**, c) **2c**, d) **2d**, e) **3a**, f) **3b** and g) **3c**. CVs were measured at a scan rate of 100 mV $s^{-1}$ in inert atmosphere using 0.1 M of $TBAPF_6$ in DMSO as supporting electrolyte and are referenced vs. $FeCp_2^{+/0}$ as an internal standard.

## 3. Optical Characterization

**Table S2.** Absorption maxima in DMSO with extinction coefficient. br = broad, sh = shoulder.

| Molecule | $\lambda_{max}$[b][nm] ($\varepsilon$[c][$dm^3\ mol^{-1}\ cm^{-1}$]) |
|---|---|
| **2a** | 385 (10100 (br)) |
| **2b** | 357 (12600), 376 (12600) |
| **2c** | 342 (10700 (sh)), 355 (11300) |
| **2d** | 357 (11300), 376 (7370 (sh)) |
| **3a** | 345 (13100 (sh)), 362 (19100), 383 (19700) |
| **3b** | 344 (12400 (sh)), 361 (18200), 381 (18900) |
| **3c** | 344 (12800 (sh)), 363 (18600), 381 (19400) |

## 4. Energy Level Diagram

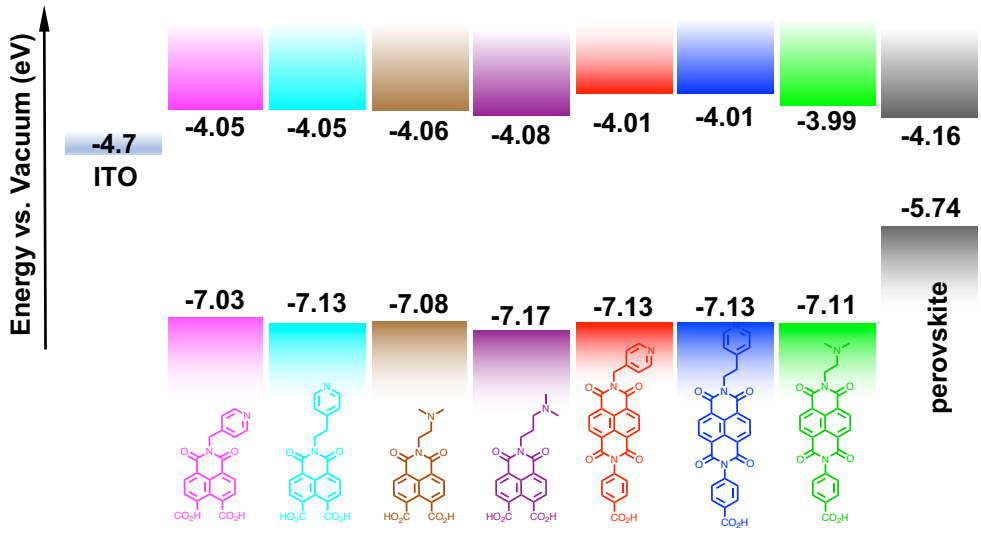


**Figure S2.** Estimated energy-level diagram of ITO and surface-modified ITOs with compounds **2a-d**, **3a-d** and $Cs_{0.05}FA_{0.79}MA_{0.16}PbI_{2.49}Br_{0.51}$

LUMO energy estimated from reduction onsets of CV measurements in DMSO vs. $FeCp_2^{+/0}$ as $E_{LUMO} = -E_{red}$(vs. $FeCp_2^{+/0}$) - 4.8 eV, $E_{HOMO} = E_{LUMO}-E_g$,
Perovskite values are taken from Lu *et al.*[1]

## 5. Self-Assembly

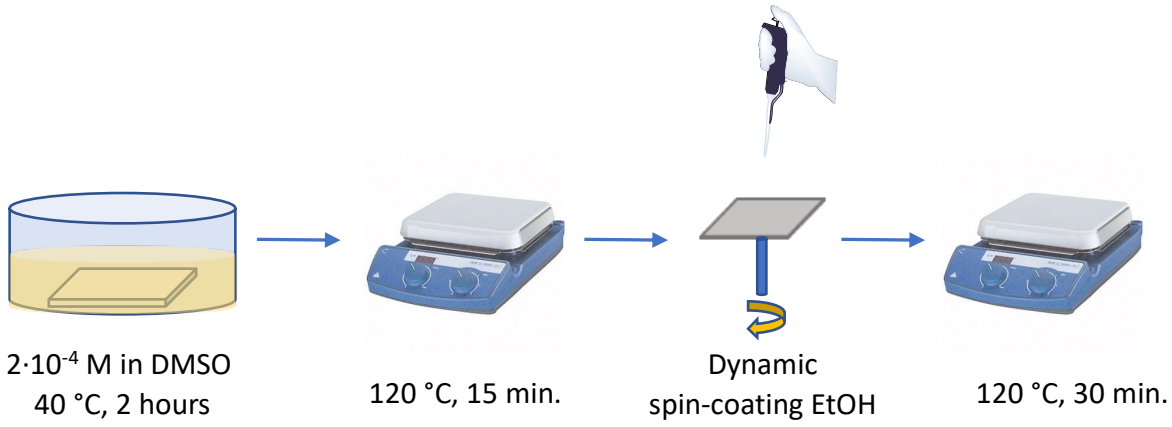


**Figure S3.** Optimized self-assembly and cleaning procedure.

ITO-coated glass substrates were cleaned in a sequence of ultrasonication baths with 2 vol% Hellmanex solution for 15 minutes followed by MilliQ water, acetone and isopropanol for 10 minutes each. The substrates were dried in a stream of nitrogen and plasma cleaned for 15 minutes to remove remaining organic residues. For the SAM deposition the freshly cleaned substrates were dipped into $2 \times 10^{-4}$ M solutions of the respective naphthalene imide in DMSO at 40 °C for 2 hours. The substrates were heated at 120 °C for 15 minutes on a hotplate and cooled down to room temperature. The films were cleaned by dynamically spin-coating 250 µl of ethanol, dried at 120 °C for 30 minutes.

## 6. Water Contact Angle Measurements

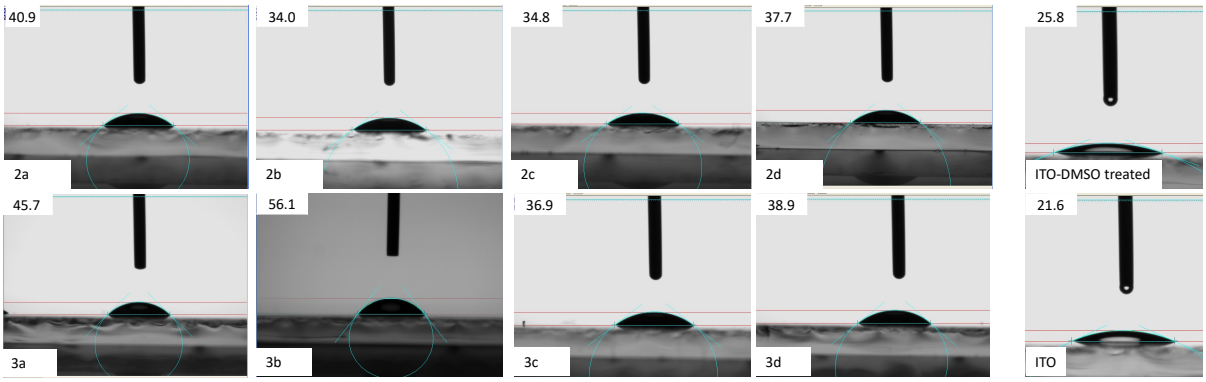


**Figure S4.** Water surface contact angles of SAM-treated ITO substrates.

**Table S3.** Water surface contact angle on ITO after treating with DMF/DMSO (4/1 v/v) and CBZ to simulate perovskite deposition.

| SAM | $\phi_C(1)$ | $\phi_C(2)$ | $\phi_C(3)$ | $\phi_C$(average) |
|---|---|---|---|---|
| 2a | 42.8 | 45.4 | 43.3 | 43.8 ±1.4 |
| 3a | 38.8 | 41.2 | 36.9 | 38.9 ±2.1 |

## 7. XPS Measurements

Synchrotron-based X-ray photoelectron spectroscopy (XPS) measurements were performed on the soft X-ray beamline at the Australian Synchrotron.[2] Samples were prepared ex-situ and no sample treatment was performed prior to measurement. Photoemission experiments were conducted at a base pressure of $10^{-10}$ mbar and measured at normal emission and the incident photon flux of X-ray was measured concurrently with each core-level using a photodiode that was moved into the X-ray beam. The four core-levels C 1s, N 1s, O 1s and In 3d were measured at photon energies 370, eV 485 eV, 620 eV and 530 eV to produce photoelectrons with kinetic energies ~85 eV to ensure similar transmission and detection probabilities. In addition, survey scans were taken on all samples to ensure there were no unexpected contaminations

The binding energy scale of all spectra were referenced to the Fermi level of a gold sample in electrical contact with the sample by establishing a $Au4f_{7/2}$ core-level binding energy of 84.0 eV. The spectra were background corrected using the Shirley method and all core-levels were fitted with Voigt function with fixed Lorentzian widths of 0.1 eV.[2] Peaks were fitted using a semi-automated approach with some constraints to peak positions, area and Gaussian widths. A summary of the XPS peak fitting including the binding energies, full width at half maximum (FWHM) and component ares is shown in Table S5.

The work function of each sample was measured using a Kelvin probe within a connected vacuum chamber. The work function of the tip was determined by measuring the contact

potential difference of a gold reference sample with known work function. The gold work function was determined from the low energy cut-off of the secondary electron measured at 170 eV with a sample bias of -9 V.[3]

**Thickness calculation**

In this work the coverage of NDI on the ITO substrates was calculated using detailed analysis of photoelectron signals from the bulk and adsorbed NDI molecules as shown in figure S5. Such analysis is not uncommon in XPS studies and has proven effective to study sub-monolayer coverages on semiconductor surfaces.[4–7]

The intensity of photoelectrons originating from the NDI layer is the product of the number of photoelectrons generated and the probability of escaping into to vacuum without elastically scattering and being detected. This is calculated from the atomic density $N_{A,2D}$, photoionisation cross section σ, the incident flux of X-rays $I_0$ and the analyser transmission and detection function $T(E)$. Subscripts A and S are used here to denote the NDI adsorbates and substrate, respectively. The photoelectron intensity originating from a core-level in the NDIs is given by:

$$I_A = xI_{0,A}N_{A,2D}\sigma_A T(E) \qquad (1)$$

Where x is the fraction area of the surface covered in molecules. We have assumed the signal from the NDI is not self-attenuated and that the NDI adsorbates directly bond to ITO substrate. A similar calculation can be performed for photoelectrons originating from the substrate:

$$I_S = xI_{0,S}N_S\lambda_S\sigma_S T(E)\exp\left(-\frac{t}{\lambda_A}\right) + (1-x)I_{0,S}N_S\lambda_S\sigma_S T(E) \qquad (2)$$

Where the first term corresponds to the signal that is attenuated by the adsorbed NDI molecules of length $t$ with inelastic mean free path (IMFP) $\lambda_A$ and the second term, to photoelectrons passing through areas of surface without adsorbates. We have assumed that photoelectrons from the substrates are self-attenuated travelling through the substrate and originate from

depths up to the substrate IMFP $\lambda_S$. The photoelectron spectra related to the substrate and adsorbates were measured at the same kinetic energy to ensure the transmission functions would cancel when taking the ratio of the two signals. A normal angle of emission was employed for both sets of measurements. By taking the ratio of the (1) and (2) and rearranging the resulting equation, the coverage of adsorbates is given by:

$$x = \frac{\left(\frac{I_A}{I_S}\right) I_{0,S} N_S \lambda_S \sigma_S}{\left(\frac{I_A}{I_S}\right) I_{0,S} N_S \lambda_S \sigma_S \left(1 - exp\left(-\frac{t}{\lambda_A}\right)\right) + I_{0,A} N_{A,2D} \sigma_A} \quad (3)$$

The coverage of NDI was determined using the N 1s signal from the NDI and In 3d signal from ITO substrates with $I_A$ and $I_S$ being the total area of the core-level peaks. The photon flux $I_0$ was measured via a photodiode moved into beam immediately before or after measurements of the corresponding core-levels. An areal density of nitrogen atoms was calculated using an expected areal density $2\times10^{14}$ NDI cm$^{-2}$ and the number of nitrogen atoms per molecule.[8,9] The bulk atomic density of In in ITO was $N_S = 3.0\times10^{22}$ cm$^{-3}$.[10] The length of each NDI was calculated based on the geometry of the molecules. The photoionisation cross sections of 3.9 and 0.49 Mbarns for In $3d_{5/2}$ and N 1s were taken from the literature.[2] The inelastic mean free path (IMFP) of photoelectrons originating from In in the ITO layer and N from the NDI were calculated using the TPP-2M method.[10] The parameters used for individual NDI molecules are given in table I.

**Table S4.** A summary of relevant parameters used to calculate the coverage of NDI on ITO substrate surfaces.

| | **2a** | **2b** | **3c** | **4d** | **3a** | **3b** | **3c** | **3d** |
|---|---|---|---|---|---|---|---|---|
| Length (nm) | 0.95 | 1.10 | 0.96 | 1.04 | 1.37 | 1.59 | 1.45 | 1.53 |
| Band gap (eV) | 4 | 4 | 4 | 4 | 4 | 4 | 4 | 4 |
| Mass density (g cm$^{-3}$) | 1 | 1 | 1 | 1 | 1 | 1 | 1 | 1 |
| IMFP (nm) | 0.59 | 0.59 | 0.59 | 0.59 | 0.58 | 0.59 | 0.59 | 0.59 |
| Areal density (molecules cm$^{-2}$) | $2\times10^{14}$ | $2\times10^{14}$ | $2\times10^{14}$ | $2\times10^{14}$ | $2\times10^{14}$ | $2\times10^{14}$ | $2\times10^{14}$ | $2\times10^{14}$ |
| N per molecule | 2 | 2 | 2 | 2 | 3 | 3 | 3 | 3 |

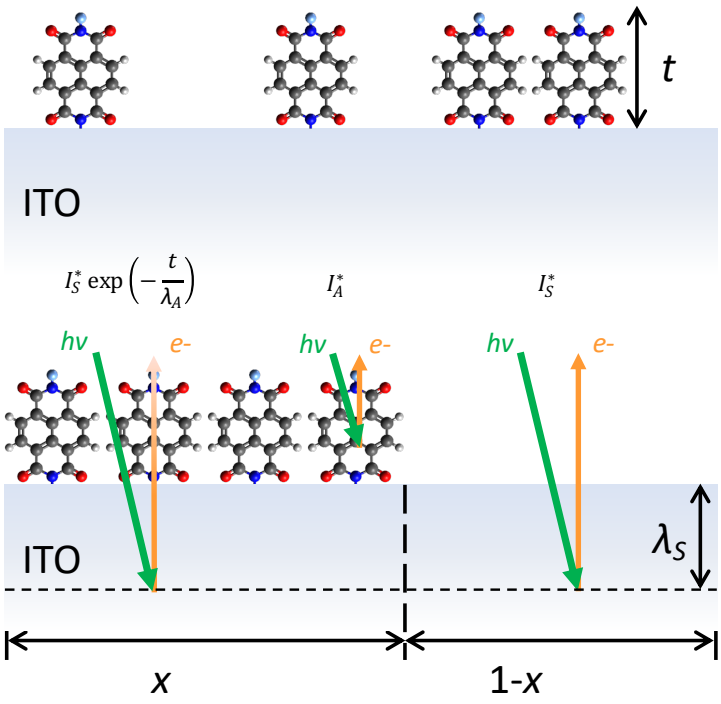


**Figure S5**. Schematic diagram showing the random arrangement of NDI adsorbates on the ITO surface with thickness *t* (top). To calculate the thickness, the surface can be divided into two effective regions, with molecules adsorbed at a relative amount of x and without molecules (bottom). The region covered with molecules produces an effective photoelectron intensity $I_A^*$ and an attenuated bulk signal of $I_S^*\exp(-t/l_A)$ while the region without molecules produces a signal $I_S^*$ from a depth of $l_S$. From the effective signals the coverage x can be calculated, see eqations 1-3 and the corresponding text for further details.

ITO

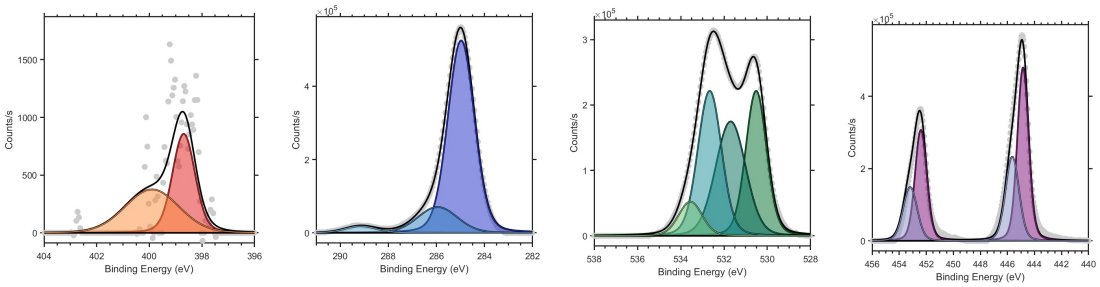


2a

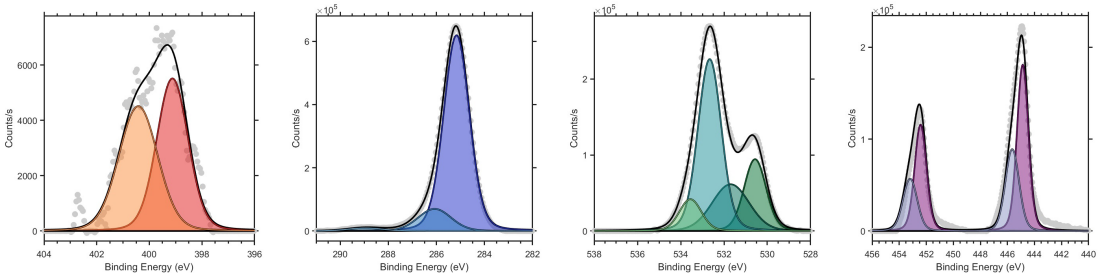


2b

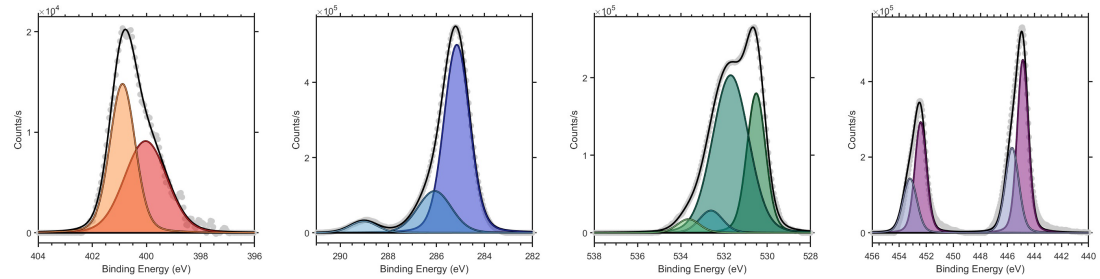


2c

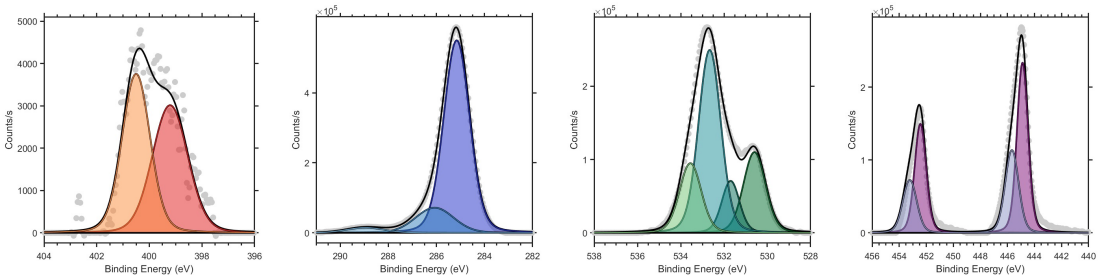


2d

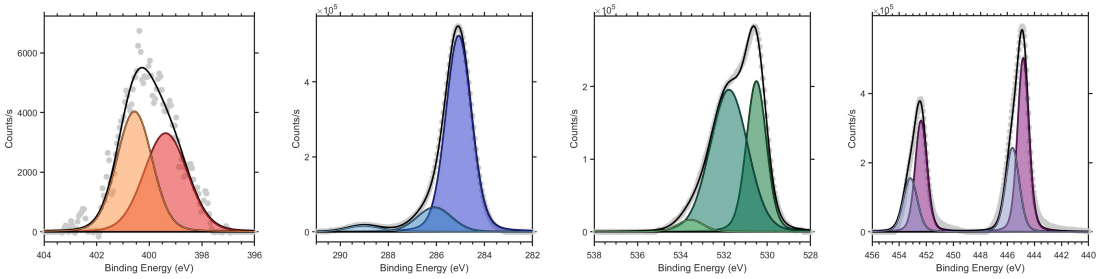


3a

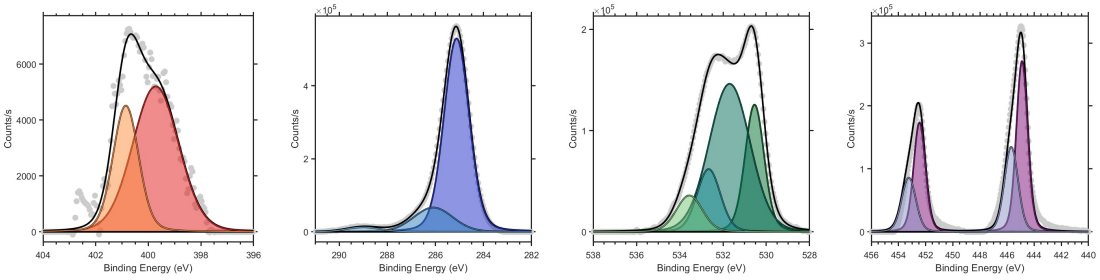

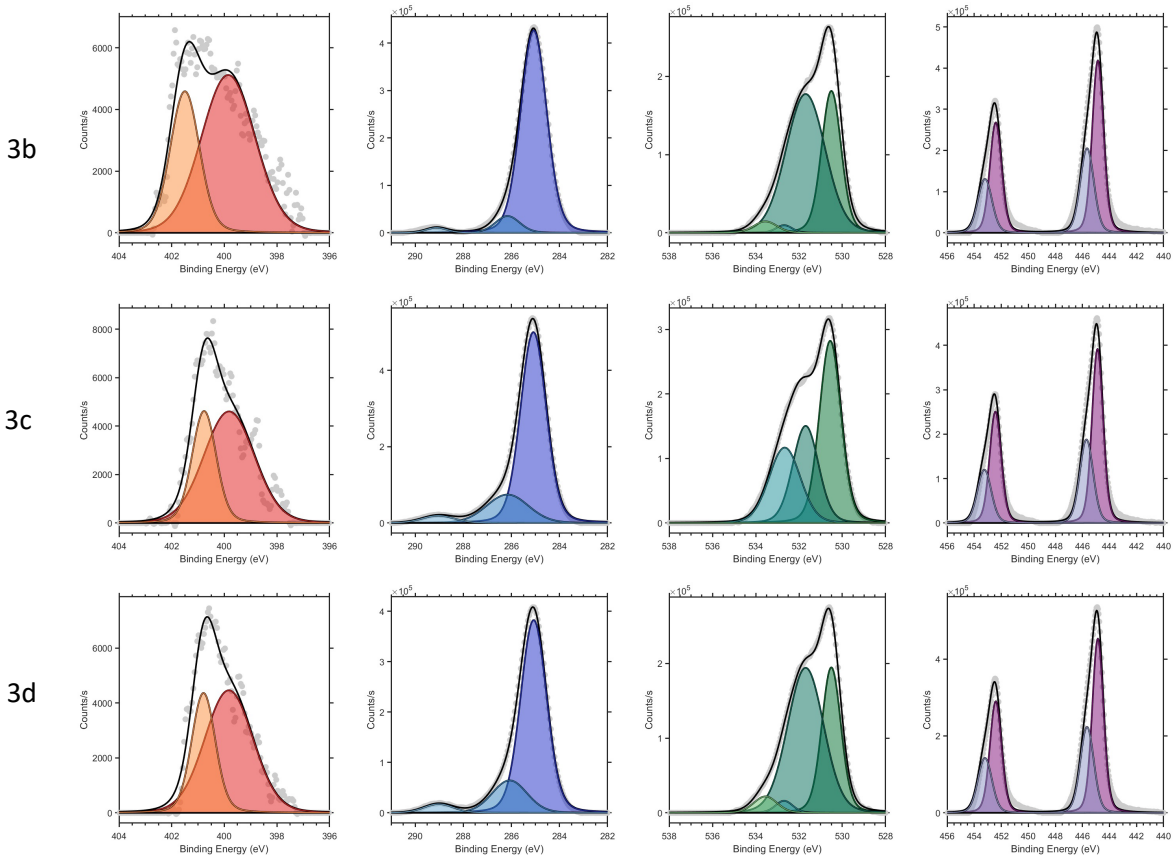


**Figure S6**. Core-level spectra N 1s, C 1s, O 1s and In 3d (left to right) for ITO with and without SAM of NDI. The list of the components and fitting details can be found in Table S4.

**Table S5.** Summary of the XPS peak fitting including the binding energies, full width at half maximum (FWHM) and component area for the C1s, N1s, In3d and O1s. Peaks are Voigt functions with fixed Lorentzian widths of 0.1 eV. For In3d, both spin orbit coupled (SOC) peaks have been included.

| Comp. | C1s | 2c | 3c | 2a | 3a | 2b | 2d | 3d | 3b | 2b | 2d | 3d | 3b | ITO | 2c | 3c | 2a | 3a | ITO |
|---|---|---|---|---|---|---|---|---|---|---|---|---|---|---|---|---|---|---|---|
| C-C, C=C, | Energy (eV) | 285.187 | 285.160 | 285.199 | 285.178 | 285.205 | 285.152 | 285.101 | 285.076 | 285.153 | 285.076 | 285.076 | 285.076 | 284.913 | 285.157 | 285.087 | 285.164 | 285.120 | 284.973 |
| C-H | FWHM (eV) | 0.593 | 0.587 | 0.614 | 0.613 | 0.607 | 0.596 | 0.622 | 0.677 | 0.632 | 0.630 | 0.637 | 0.640 | 0.647 | 0.635 | 0.629 | 0.631 | 0.617 | 0.649 |
| | Area | 492126 | 702771 | 687933 | 582658 | 663232 | 730892 | 806153 | 412673 | 714285 | 746236 | 551182 | 617777 | 630629 | 789776 | 712623 | 883801 | 740211 | 769756 |
| C-O, C-N | Energy (eV) | 286.120 | 286.047 | 286.119 | 286.120 | 286.079 | 286.108 | 286.076 | 286.164 | 286.076 | 286.084 | 286.076 | 286.164 | 285.824 | 286.076 | 286.164 | 286.076 | 286.090 | 285.952 |
| | FWHM (eV) | 1.129 | 0.932 | 0.924 | 1.066 | 0.884 | 0.955 | 0.906 | 0.887 | 0.825 | 0.845 | 0.853 | 0.599 | 0.936 | 0.929 | 1.025 | 0.805 | 0.954 | 0.964 |
| | Area | 326146 | 209800 | 238154 | 289194 | 303215 | 205104 | 165840 | 72880 | 204391 | 123131 | 122291 | 48222 | 108658 | 147942 | 168636 | 125623 | 140431 | 150400 |
| C=O, OH-C=O, | Energy (eV) | 289.030 | 289.110 | 289.066 | 289.068 | 289.030 | 289.110 | 289.026 | 289.114 | 289.026 | 289.026 | 289.026 | 289.114 | 289.213 | 288.956 | 289.044 | 288.956 | 289.003 | 289.152 |
| N-C=O, | FWHM (eV) | 0.731 | 0.753 | 0.701 | 0.778 | 0.641 | 0.769 | 0.823 | 0.696 | 0.668 | 0.816 | 0.732 | 0.525 | 0.692 | 0.930 | 0.797 | 0.863 | 0.823 | 0.772 |
| Shake up | Area | 80048 | 40479 | 60189 | 61853 | 69614 | 41064 | 30539 | 21378 | 46411 | 30377 | 28613 | 12986 | 16187 | 30286 | 33965 | 17816 | 23382 | 31495 |

| Comp. | N1s | 2c | 3c | 2a | 3a | 2b | 2d | 3d | 3b | 2b | 2d | 3d | 3b | ITO | 2c | 3c | 2a | 3a | ITO |
|---|---|---|---|---|---|---|---|---|---|---|---|---|---|---|---|---|---|---|---|
| C-N, | Energy (eV) | 400.143 | 398.978 | 399.718 | 399.306 | 400.047 | 399.380 | 398.836 | 398.843 | 400.029 | 399.381 | 399.267 | 399.040 | 400.021 | 399.214 | 399.208 | 399.124 | 399.222 | 398.696 |
| Pyridinic N | FWHM (eV) | 0.893 | 1.204 | 0.894 | 0.728 | 0.980 | 0.851 | 1.162 | 1.072 | 0.925 | 0.972 | 0.731 | 1.014 | 1.115 | 0.794 | 0.823 | 0.705 | 0.695 | 0.504 |
| | Area | 18475 | 5313 | 15723 | 7350 | 22539 | 4716 | 3982 | 3558 | 18682 | 7104 | 5248 | 7004 | 4829 | 5340 | 5696 | 8728 | 5891 | 993 |
| N-C=O | Energy (eV) | 400.977 | 400.587 | 400.906 | 400.672 | 400.956 | 400.528 | 400.348 | 400.265 | 400.882 | 400.565 | 400.635 | 401.061 | 401.579 | 400.504 | 400.619 | 400.422 | 400.616 | 399.900 |
| | FWHM (eV) | 0.620 | 0.885 | 0.609 | 0.680 | 0.576 | 0.609 | 0.792 | 1.049 | 0.553 | 0.789 | 0.675 | 1.027 | 0.873 | 0.628 | 0.703 | 0.871 | 0.774 | 1.204 |
| | Area | 18490 | 10591 | 15731 | 14698 | 22552 | 4714 | 7929 | 7096 | 18690 | 7101 | 10493 | 14014 | 4847 | 5337 | 11386 | 8723 | 11781 | 992 |

| Comp. | In3d | 2c | 3c | 2a | 3a | 2b | 2d | 3d | 3b | 2b | 2d | 3d | 3b | ITO | 2c | 3c | 2a | 3a | ITO |
|---|---|---|---|---|---|---|---|---|---|---|---|---|---|---|---|---|---|---|---|
| $In_2O_3$ | Energy (eV) | 444.910 | 444.902 | 444.811 | 444.849 | 444.860 | 444.862 | 444.838 | 444.828 | 444.866 | 444.838 | 444.861 | 444.861 | 444.824 | 444.886 | 444.886 | 444.873 | 444.899 | 444.852 |
| $In3d_{5/2}$ | FWHM (eV) | 0.522 | 0.491 | 0.493 | 0.494 | 0.497 | 0.498 | 0.487 | 0.502 | 0.492 | 0.494 | 0.493 | 0.497 | 0.500 | 0.487 | 0.487 | 0.500 | 0.496 | 0.491 |
| | Area | 517480 | 445662 | 502964 | 589302 | 437047 | 553788 | 439277 | 679581 | 518302 | 572632 | 514785 | 479360 | 309015 | 262604 | 440460 | 208139 | 310185 | 543634 |
| (SOC) $In3d_{3/2}$ | Energy (eV) | 452.460 | 452.452 | 452.361 | 452.399 | 452.410 | 452.412 | 452.388 | 452.378 | 452.416 | 452.388 | 452.411 | 452.411 | 452.374 | 452.436 | 452.436 | 452.423 | 452.449 | 452.402 |
| | FWHM (eV) | 0.542 | 0.510 | 0.513 | 0.514 | 0.517 | 0.518 | 0.507 | 0.522 | 0.511 | 0.514 | 0.513 | 0.517 | 0.520 | 0.507 | 0.507 | 0.520 | 0.516 | 0.511 |
| | Area | 342604 | 295936 | 333916 | 391185 | 290034 | 367479 | 291789 | 450729 | 344126 | 380110 | 341746 | 318096 | 204999 | 174443 | 292580 | 138083 | 205857 | 360958 |

| | | | | | | | | | | | | | | | | | | | |
|---|---|---|---|---|---|---|---|---|---|---|---|---|---|---|---|---|---|---|---|
| In(OH)x, | Energy (eV) | 445.698 | 445.709 | 445.610 | 445.650 | 445.646 | 445.660 | 445.632 | 445.632 | 445.659 | 445.633 | 445.662 | 445.660 | 445.605 | 445.672 | 445.704 | 445.648 | 445.694 | 445.647 |
| InOOH | FWHM (eV) | 0.622 | 0.590 | 0.592 | 0.594 | 0.596 | 0.597 | 0.587 | 0.602 | 0.591 | 0.593 | 0.592 | 0.597 | 0.600 | 0.586 | 0.587 | 0.599 | 0.596 | 0.591 |
| $In3d_{5/2}$ | Area | 272560 | 255434 | 285212 | 326686 | 249666 | 313270 | 255608 | 382192 | 301965 | 328040 | 301155 | 278332 | 179600 | 151748 | 250862 | 121215 | 182556 | 313292 |
| (SOC) $In3d_{3/2}$ | Energy (eV) | 453.248 | 453.259 | 453.160 | 453.200 | 453.196 | 453.210 | 453.182 | 453.182 | 453.209 | 453.183 | 453.212 | 453.210 | 453.155 | 453.222 | 453.254 | 453.198 | 453.244 | 453.197 |
| | FWHM (eV) | 0.641 | 0.610 | 0.612 | 0.614 | 0.616 | 0.617 | 0.607 | 0.622 | 0.611 | 0.613 | 0.612 | 0.617 | 0.620 | 0.606 | 0.607 | 0.619 | 0.615 | 0.611 |
| | Area | 179120 | 168202 | 187785 | 215073 | 164336 | 206191 | 168351 | 251468 | 198823 | 215958 | 198272 | 183195 | 118189 | 99949 | 165226 | 79769 | 120165 | 206287 |

| **Comp.** | **O1s** | **2c** | **3c** | **2a** | **3a** | **2b** | **2d** | **3d** | **3b** | **2b** | **2d** | **3d** | **3b** | **ITO** | **2c** | **3c** | **2a** | **3a** | **ITO** |
|---|---|---|---|---|---|---|---|---|---|---|---|---|---|---|---|---|---|---|---|
| $In_2O_3$ (bulk) | Energy (eV) | 530.551 | 530.570 | 530.506 | 530.538 | 530.537 | 530.534 | 530.506 | 530.516 | 530.515 | 530.506 | 530.508 | 530.508 | 530.506 | 530.594 | 530.560 | 530.567 | 530.546 | 530.517 |
| | FWHM (eV) | 0.500 | 0.515 | 0.562 | 0.519 | 0.515 | 0.511 | 0.519 | 0.573 | 0.512 | 0.546 | 0.523 | 0.534 | 0.585 | 0.603 | 0.591 | 0.600 | 0.519 | 0.567 |
| | Area | 217648 | 222263 | 311972 | 289721 | 214450 | 240741 | 259524 | 380609 | 211249 | 258264 | 232931 | 221097 | 225226 | 150340 | 378337 | 128311 | 149176 | 285833 |
| $In(OH)_x$ | Energy (eV) | 531.696 | 531.696 | 531.696 | 531.696 | 531.759 | 531.696 | 531.696 | 531.696 | 531.696 | 531.775 | 531.696 | 531.696 | 531.696 | 531.696 | 531.696 | 531.696 | 531.696 | 531.696 |
| | FWHM (eV) | 1.018 | 1.036 | 0.802 | 1.049 | 1.046 | 1.104 | 1.098 | 0.781 | 0.985 | 1.028 | 0.982 | 1.065 | 0.791 | 0.484 | 0.702 | 1.007 | 1.116 | 0.817 |
| | Area | 547682 | 477763 | 402473 | 629749 | 502828 | 544370 | 562711 | 399925 | 441414 | 442434 | 420372 | 415001 | 235179 | 78947 | 236870 | 136273 | 357838 | 317684 |
| O=C | Energy (eV) | 532.668 | 532.694 | 532.687 | 532.694 | 532.606 | 532.694 | 532.694 | 532.694 | 532.606 | 532.606 | 532.694 | 532.694 | 532.660 | 532.664 | 532.664 | 532.664 | 532.664 | 532.664 |
| | FWHM (eV) | 0.678 | 0.577 | 0.593 | 0.403 | 0.644 | 0.447 | 0.473 | 0.567 | 0.639 | 0.552 | 0.474 | 0.440 | 0.640 | 0.607 | 0.855 | 0.638 | 0.637 | 0.645 |
| | Area | 43071 | 28266 | 86422 | 5897 | 23565 | 8862 | 20304 | 89001 | 41436 | 0 | 17620 | 10025 | 279115 | 342843 | 221662 | 325510 | 89003 | 321931 |
| O-C, HO-C, | Energy (eV) | 533.644 | 533.573 | 533.556 | 533.556 | 533.644 | 533.556 | 533.556 | 533.556 | 533.644 | 533.556 | 533.556 | 533.556 | 533.556 | 533.556 | - | 533.556 | 533.556 | 533.556 |
| $H_2O$ | FWHM (eV) | 0.722 | 0.616 | 0.648 | 0.688 | 0.678 | 0.605 | 0.658 | 0.572 | 0.612 | 0.692 | 0.632 | 0.631 | 0.613 | 0.593 | - | 0.602 | 0.708 | 0.640 |
| | Area | 35515 | 28586 | 48873 | 41684 | 24043 | 23854 | 45397 | 35847 | 24451 | 25940 | 31391 | 20815 | 59459 | 127648 | - | 57001 | 56973 | 75351 |

XPS peak fitting references: Lopez *et al.*,[11] Meyer *et al.*,[12] Idriss *et al.*,[13] Smets *et al.*,[14] Frath *et al.*,[15] Schenk *et al.*,[16] Chastain *et al.*,[17] Wang *et al.*,[18] Detweiler and Wulfsberg *et al.*,[19] Donley *et al.*[20]

## 8. Perovskite Solar Cells

### Precursor Materials and Preparation

All chemicals were purchased from Sigma Aldrich and used as received unless stated otherwise. Lead(II) iodide (ultradry, 99.999% metal basis), lead(II) bromide (ultradry, 99.999% metal basis), and caesium iodide (99.999%) were purchased from Alfa Aesar. Formamidinium iodide (FAI) (99.99%) and methylammonium bromide (MABr) (99.99%) were purchased from Greatcell Solar Ltd. 2,2′,7,7′-Tetrakis(N,N-di-p-methoxyphenyl-amine)-9,9′-spirobifluorene (spiro-OMeTAD) was purchased from Luminescence Technology Corp. Glass substrates 2.5 cm × 2.5 cm coated with ITO (15 Ω $sq^{-1}$ sheet resistance) and laser engraved to make four individual devices were purchased from Yingkou Shangneng Photoelectric material Co., Ltd. $[Cu(dmp)_2][TFSI]_2$ dopant was synthesized as previously reported.[21]

In a glove box 189.2 mg FAI, 557.8 mg $PbI_2$, 80.7 mg $PbBr_2$ and 24.6 mg MABr were dissolved in 1 ml of a mixture of N,N-dimethylformamide (DMF) and dimethyl sulfoxide (DMSO) (4:1 v/v). 47.7 µl of a 1.5 M solution of CsI in DMSO was added and the perovskite precursor was shaken for 10 minutes until fully dissolved. For the hole-transporting material (HTM) solution 72.3 mg spiro-OMeTAD were mixed with 1 ml of chlorobenzene (CBZ), 28.8 µl of of 4-*tert*-butylpyridine and 17.5 µl of LiTFSI in acetonitrile (MeCN; 520 mg in 1 ml). The mixture was shaken for 1 min until fully dissolved. Spiro-OMeTAD was doped by adding 18 µl of a solution of $[Cu(dmp)_2][TFSI]_2$ in MeCN (7.8 mg in 30 µl) were added.

### Perovskite Cell and Thin Film Fabrication

Pre-patterned ITO-coated glass substrates were cleaned in a sequence of ultrasonication baths with 2 vol% Hellmanex solution for 15 minutes followed by MilliQ water, acetone and isopropanol for 10 minutes each. The substrates were dried in a stream of nitrogen and plasma cleaned for 15 minutes to remove remaining organic residues. For the SAM deposition the

freshly cleaned substrates were dipped into $2 \times 10^{-4}$ M solutions of the respective naphthalene imide in DMSO at 40 °C for 2 hours. The substrates were heated at 120 °C for 15 minutes on a hotplate and cooled down to room temperature. The films were cleaned by dynamically spin-coating 250 µl of ethanol, dried at 120 °C for 30 minutes and immediately transferred to the glove box for the perovskite deposition. 35 µL of perovskite precursor solution was spread onto the substrates and spin-coated following a two-step program at 1000 rpm with an acceleration of 1000 rpm $s^{-1}$ for 10 s followed by 6000 rpm with an acceleration of 6000 rpm $s^{-1}$ for 20 s. 200 µL of chlorobenzene was poured onto the substrate 5 s prior to the end of the second step. The films were annealed at 100 °C for 30 minutes. After cooling to room temperature, the HTM solution (35 µL) was dynamically spin-coated at 2000 rpm for 30 s. Perovskite was removed at the edges of the substrate using a cotton swab dipped in a solvent mixture of DMF/IPA/CBZ (1:1:1 v/v). Finally, an 80 nm thick Au electrode was thermally evaporated onto the HTM layer.

Current–voltage characteristics were measured using a high-throughput set up as described previously.[22] The devices were measured at 100 mW $cm^{-2}$ using a Keithley source meter, an Abet Technologies Sun 3000 class AAA solar simulator equipped with a an AM 1.5G filter and were calibrated with a Si-reference cell. A nonreflective metal aperture of 0.16 $cm^2$ was used to define the irradiation area. The J–V scans were conducted with a scan rate of 100 mV $s^{-1}$ at 10 mV steps with settling times of 100 ms (0.1 V s−1) both in reverse (1.2 V → −0.2 V) and forward (−0.2 V → 1.2 V) scan directions. The devices were light-soaked for 10 s prior to scanning. The stabilized efficiency of the devices was conducted by holding the potential corresponding to the maximum power point of the reverse scan. Incident photon to current efficiency spectra were recorded using a Keithley 2400 Source Meter combined with irradiation form a 300 W xenon lamp and an Oriel Corner-stone 260¼m monochromator. The

monochromatic photon flux was quantified with a calibrated silicon cell (Peccell Technologies).

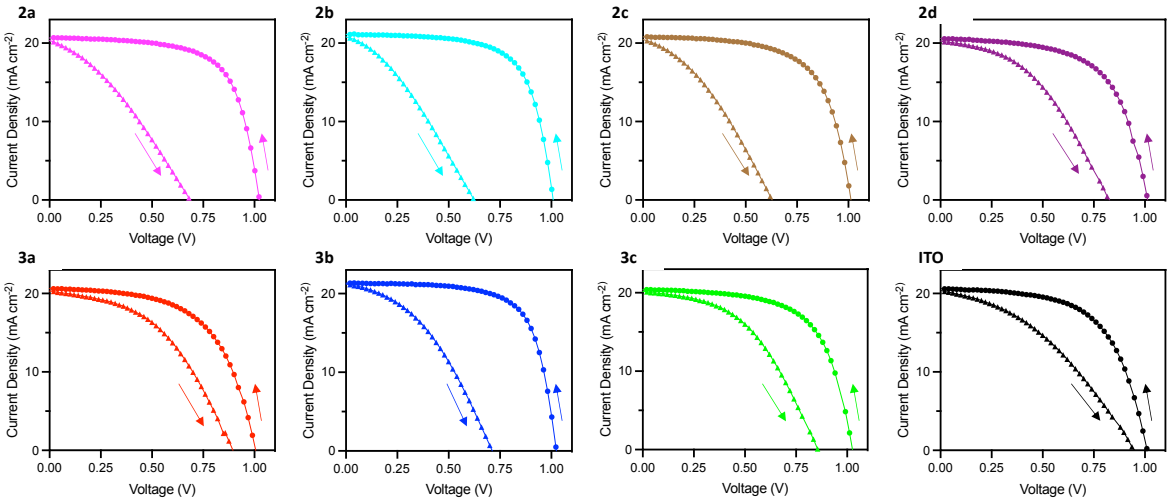


**Figure S7**. Forward and reverse scans of champion devices.

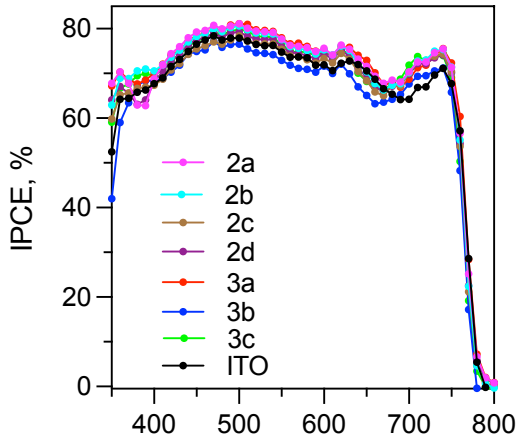


**Figure S8**. Incident photon to current efficiency (IPCE) spectra of the champion devices.

## 9. Surface Recombination Velocity Measurements

Surface Recombination Velocity (SRV) was analyzed based on transient photoluminescence (TRPL) data following a method published previously.[23] The TRPL was measured using a PicoQuant Picoharp 300 TCSPC system equipped with a 470 nm pulsed diode laser (PDL-800 LDH-P-C-470B, 300 ps pulse width). The laser was pulsed at repetition rates from 100 KHz to 1 MHz. The PL emission was filtered using a 580 nm long-pass filter before being directed to the detector.

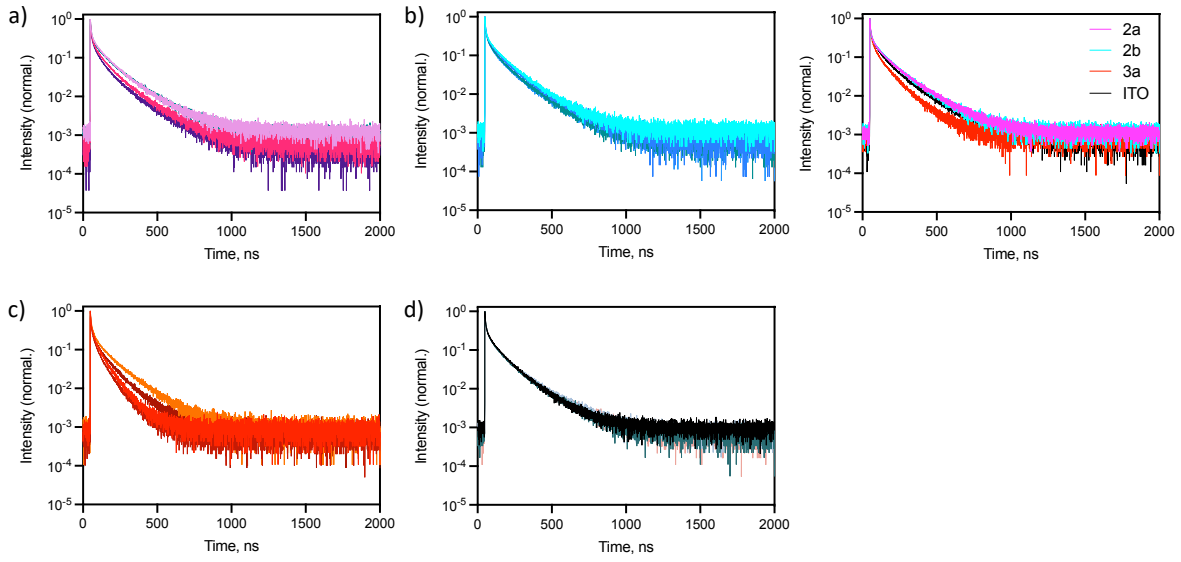


**Figure S9.** Transient photoluminescence decays of perovskite films in contact with a) **2a**/ITO, b) **2b**/ITO, c) **3a**/ITO and d) ITO.

## 10. Drift-Diffusion Simulations

Solar Cell Capacitance Simulator (SCAPS) was used for the drift-diffusion simulations with a device structure of ITO|perovskite|spiro-OMeTAD. While NDIs were not included as a discrete film in the simulations, the impact of NDI on the device performance was simulated by tuning the SRV and work function of the ITO layer over range of $10^{-2}$ to $10^{6}$ cm $s^{-1}$ and 4.0 to 5.2 eV, respectively. The parameters used for the simulation at summarised in Table S6 and were chosen to give good agreement with our experimental results and simulations published elsewhere.[23–25] The bulk carrier lifetimes in the bulk were set equally to 2 µs. We set the SRV of spiro-OMeTAD to $5\times10^{3}$ cm $s^{-1}$ and a 0.25 eV offset for the perovskite and spiro-OMeTAD valence band and assumed the flat band condition at the back contact. The optical absorption coefficient spectrum of the perovskite layer was taken from elsewhere and we assumed a 20% optical transmission lost through the ITO layer.[26] The work function of the back contact (adjacent to the spiro-OMeTAD layer) matched that of spiro-OMeTAD *i.e.*, the flat band condition. The extraction velocities of majority carriers at the electrodes have been set to $10^{7}$ cm/s.

**Table S6.** A summary of relevant parameters used for the drift-diffusion simulations.

| | Perovskite | Spiro-OMeTAD |
|---|---|---|
| Thickness (nm) | 500 | 200 |
| Band gap (eV) | 1.6 | 3 |
| Electron affinity (eV) | 4.15 | 2.50 |
| Dielectric permittivity | 22 | 3 |
| CB effective density of states ($cm^{-3}$) | $2.0\times10^{18}$ | $1.0\times10^{20}$ |
| VB effective density of states ($cm^{-3}$) | $2.0\times10^{18}$ | $1.0\times10^{20}$ |
| Thermal velocity of electrons, holes (cm $s^{-1}$) | $1.0\times10^{7}$ | $1.0\times10^{7}$ |
| Band to band recombination rate $cm^3$ $s^{-1}$ | $6.0\times10^{-11}$ | 0 |
| Electron mobility ($cm^2$ $V^{-1}$ $s^{-1}$) | 2 | $1.0\times10^{-4}$ |
| Hole mobility ($cm^2$ $V^{-1}$ $s^{-1}$) | 2 | $1.0\times10^{-4}$ |
| Shallow donor density ND ($cm^{-3}$) | $1.0\times10^{10}$ | 0 |
| Shallow acceptor density NA ($cm^{-3}$) | $1.0\times10^{10}$ | $1.0\times10^{18}$ |
| Electron, hole Lifetimes (ns) | 2000 | 1 |

## 11. Shelf-Life Stability

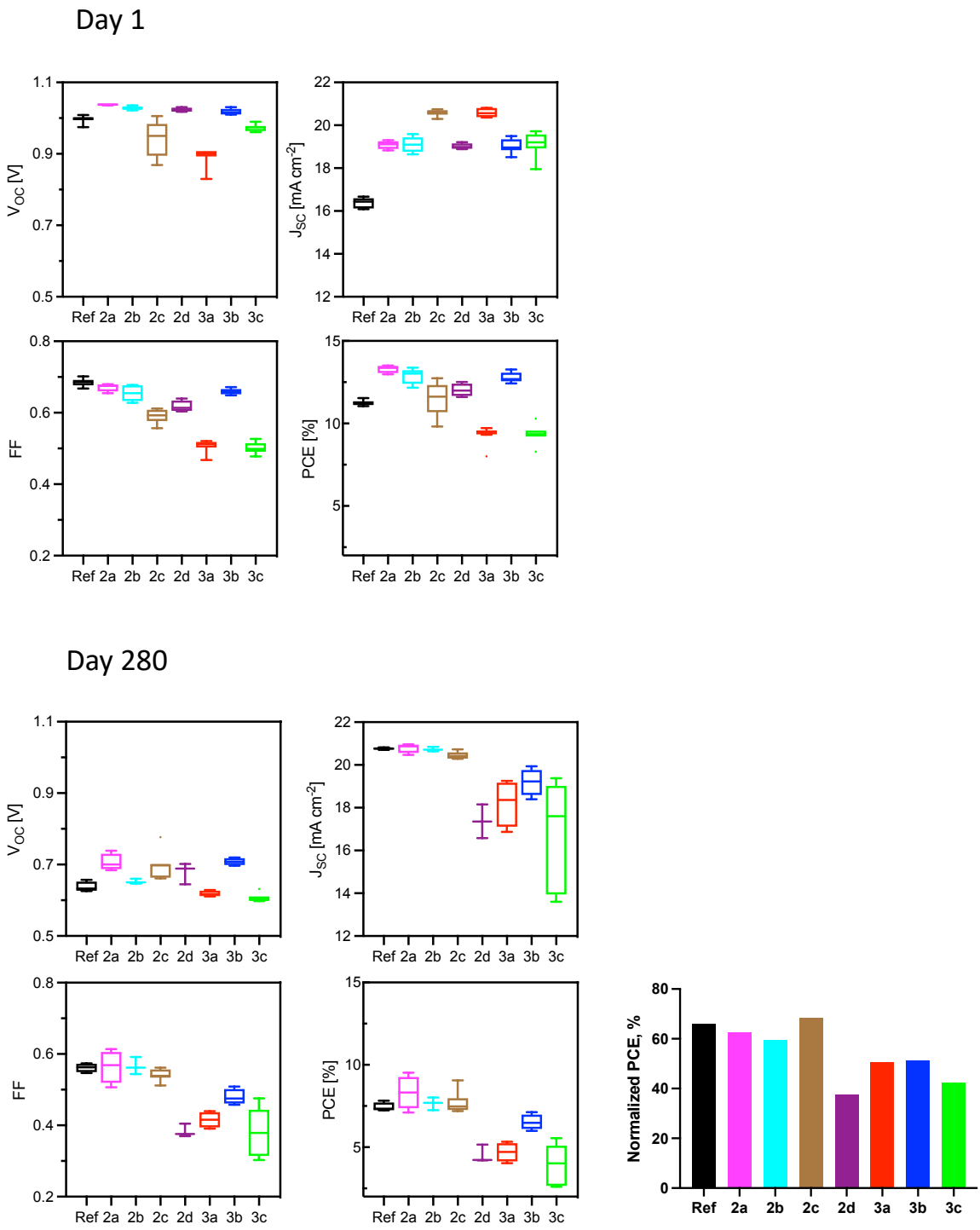


**Figure S10.** Shelf-life stability. Top: Photovoltaic parameters on the day of fabrication. Bottom: Photovoltaic parameters on the day 280 after fabrication and the normalized PCE on day 280.

## 12. Synthesis

### 12.1. Naphthalene monoimides 2a-2d

1,4,5,8-naphthalenetetracarboxylic dianhydride (2.00 g, 7.46 mmol) was reacted with KOH (1.96 g, 35.0 mmol) in 230 ml water to form a yellow solution of the potassium carboxylate. The pH was adjusted to 6.5 with $H_3PO_4$ (40% in $H_2O$) to form the monoanhydride. 1 eq of the respective amine was added, the pH readjusted to 6.5 and the solution was refluxed for 24 h in an atmosphere of nitrogen. After cooling to room temperature the solution was filtered and the filtrate acidified to form a fine suspension that was filtered and washed with water, methanol and diethyl ether. The off-white powder was dried *in vacuo*.

**NMI-2a**

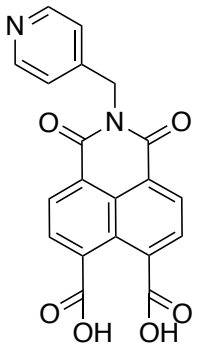


Yield: 83.1 %.

$^1$H NMR (400 MHz, DMSO-$d_6$ + $D_2SO_4$) δ / ppm: 8.82 (m, 2H), 8.52 (d, $J$ = 7.7 Hz, 2H), 8.17 (d, $J$ = 7.2 Hz, 2H), 8.12 (d, $J$ = 6.0 Hz, 2H), 5.46 (s, 2H). $^{13}$C{$^1$H} NMR (100 MHz, DMSO-$d_6$ + $D_2SO_4$) δ / ppm: 98.8, 163.6, 158.6, 142.0, 137.2, 130.9, 129.8, 129.5, 126.0, 125.6, 125.2, 43.8. HRMS (ESI) m/z: 375.0621 $[M-H]^-$ (calc. 375.0623). $T_d$: 177 °C.

**NMI-2b**

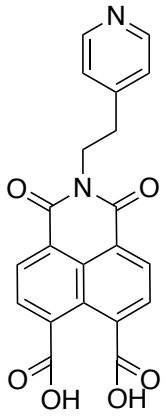

Yield: 74.1 %.

$^{1}$H NMR (400 MHz, DMSO-$d_6$ + $D_2SO_4$) δ / ppm: 8.76 (d, *J* = 6.7 Hz, 2H), 8.47 (d, *J* = 7.6 Hz 2H), 8.14 (d, *J* = 7.6 Hz, 2H), 8.01 (d, *J* = 6.8 Hz, 2H), 4.36 (t, *J* = 6.8 Hz, 2H), 3.25 (t, *J* = 6.7 Hz, 2H). $^{13}$C{$^{1}$H} NMR (100 MHz, DMSO-$d_6$ + $D_2SO_4$) δ / ppm: 169.8, 164.2, 162.1, 142.3, 137.8, 131.8, 130.8, 129.9, 129.1, 126.7, 125.8, 124.9, 35.07. HRMS (EI) m/z: 391.0926 $[M+H]^+$ (calc. 391.0925). $T_d$: 219 °C.

**NMI-2c**

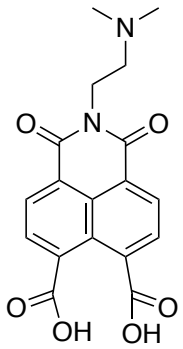

Yield: 51.9 %.

$^{1}$H NMR (400 MHz, DMSO-$d_6$ + $D_2SO_4$) δ / ppm: 8.55 (m, 2H), 8.19 (m, 2H), 4.35 (m, 2H), 3.45 (t\m, 2H), 2.89 (s, 6H). $^{13}$C{$^{1}$H} NMR (100 MHz, DMSO-$d_6$ + $D_2SO_4$) δ / ppm: 163.5, 136.9, 130.4, 129.4, 128.8, 125.6, 124.8, 54.9, 42.9, 35.5. HRMS (ESI) m/z: 355.0932 $[M-H]^-$ (calc. 355.0936). $T_d$: 186 °C.

**NMI-2d**

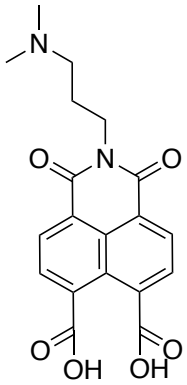


Yield: 18.0 %.

$^{1}$H-NMR (400 MHz, $D_2SO_4$) δ / ppm: 9.59 (d, *J* = 7.7 Hz, 2H), 9.53 (d, *J* = 7.8 Hz, 2H), 4.99 (m, 2H), 3.89 (m, 2H), 3.53 (d, *J* = 5.1 Hz, 6H), 2.89 (m, 2H). HRMS (ESI) m/z: 369.1090 $[M-H]^-$ (calc. 369.1092). $T_d$: 202 °C.

## 12.2. Naphthalene diimides 3a-3d

The appropriate monoimide (3.72 mmol) and 4-aminobenzoic acid (5.59 mmol) were suspended in dry DMF and was heated in a microwave reactor with 300 W to 75 °C for 5 min, then for 45 min. at 140 °C at 250 psi. The mixture was poured into water and the precipitate filtered and washed with water and methanol. The light brown powder was dried in vacuo.

**NDI-3a**

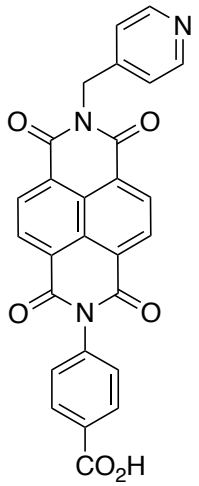


Yield: 33.0 %.

$^{1}$H NMR (400 MHz, DMSO-$d_6$ + $D_2SO_4$) δ / ppm: 8.76 (m, 2H), 8.64 (d, *J* = 7.7 Hz, 2H), 8.61 (d, *J* = 7.7 Hz, 2H), 8.10 (d, *J* = 7.0 Hz, 2H), 8.01 (m, 2H), 7.51 (d, *J* = 8.5 Hz, 2H), 5.45 (s, 2H). $^{13}$C{$^{1}$H} NMR (100 MHz, DMSO-$d_6$ + $D_2SO_4$) δ / ppm: 167.2, 163.5, 163.2, 158.4, 142.0, 140.1, 131.3, 131.2, 131.0, 130.5, 129.9, 127.4, 127.2, 127.1, 127.0, 125.7, 43.9. HRMS (EI) m/z: 477.0953 $[M]^+$ (calc. 477.0961). $T_d$: 365 °C.

**NDI-3b**

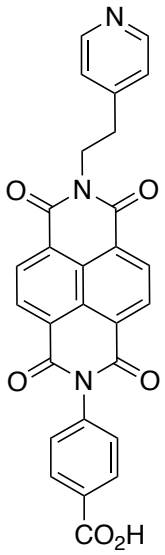

Yield: 6.0 %.

$^1$H-NMR (400 MHz, $D_2SO_4$) δ / ppm: 9.61(m, 4H), 9.25 (m, 2H), 9.17 (m, 2H), 8.69 (d, *J* = 6.3 Hz, 2H), 8.42 (d, *J* = 8.3 Hz, 2H), 5.31 (m, 2H), 4.11 (m, 2H). ESI, $[M+H]^+$: 492.1186 (calc. 492.1190). $T_d$: 308 °C.

**NDI-3c**

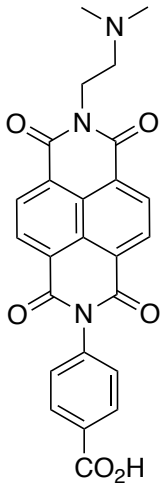

Yield: 67.0 %.

$^1$H NMR (400 MHz, DMSO-$d_6$ + $D_2SO_4$) δ / ppm: 8.65 (d, *J* = 7.6 Hz, 2H), 8.61 (d, *J* = 7.6 Hz, 2H), 8.02 (d, *J* = 8.5 Hz, 2H), 7.52 (d, *J* = 8.5 Hz, 2H), 4.33 (m, 2H), 3.44 (m, 2H), 2.87 (s, 6H). HRMS (ESI) m/z: 458.1342 $[M+H]^+$ (calc. 458.1347). $T_d$: 324 °C.

**NDI-3d**

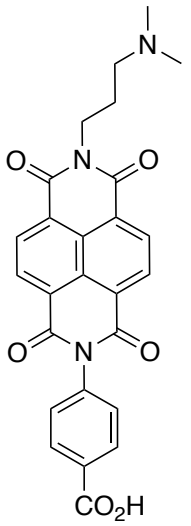


$^1$H NMR (400 MHz, DMSO-$d_6$) δ / ppm: 8.70 (m, 4H), 8.06 (d, *J* = 8.5 Hz, 2H), 7.54 (d, *J* = 8.5 Hz, 2H), 4.12 (t, *J* = 7.4 Hz, 2H), 2.45 (t, *J* = 7.0 Hz, 2H), 2.21 (s, 6H), 1.85 (quint., *J* = 7.2 Hz, 2H). ESI-MS m/z: 472.2 $[M+H]^+$ (calc. 472.14). $T_d$: 323 °C.

## 13. NMR Spectra

### NMI-2a

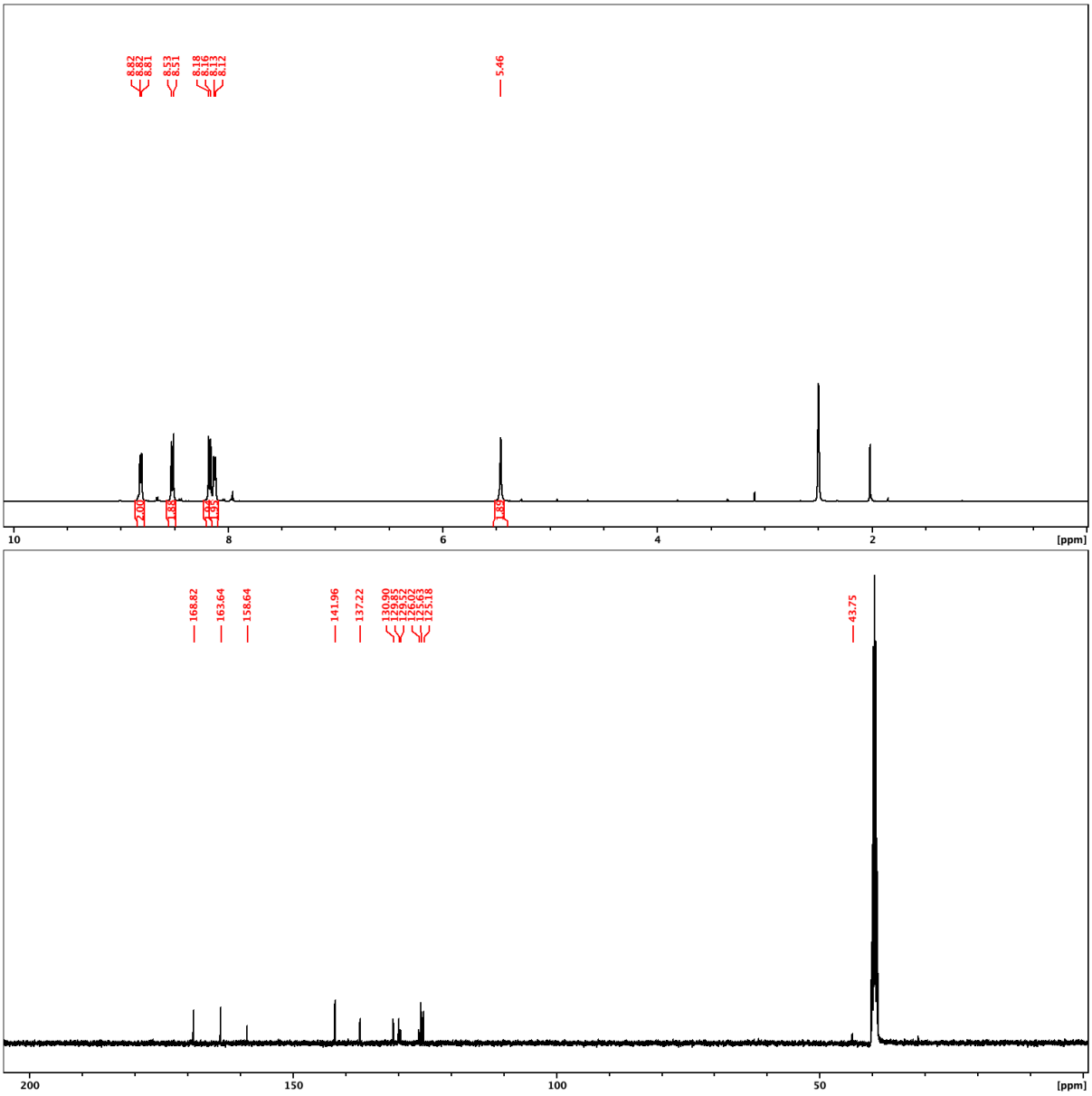


### NMI-2b

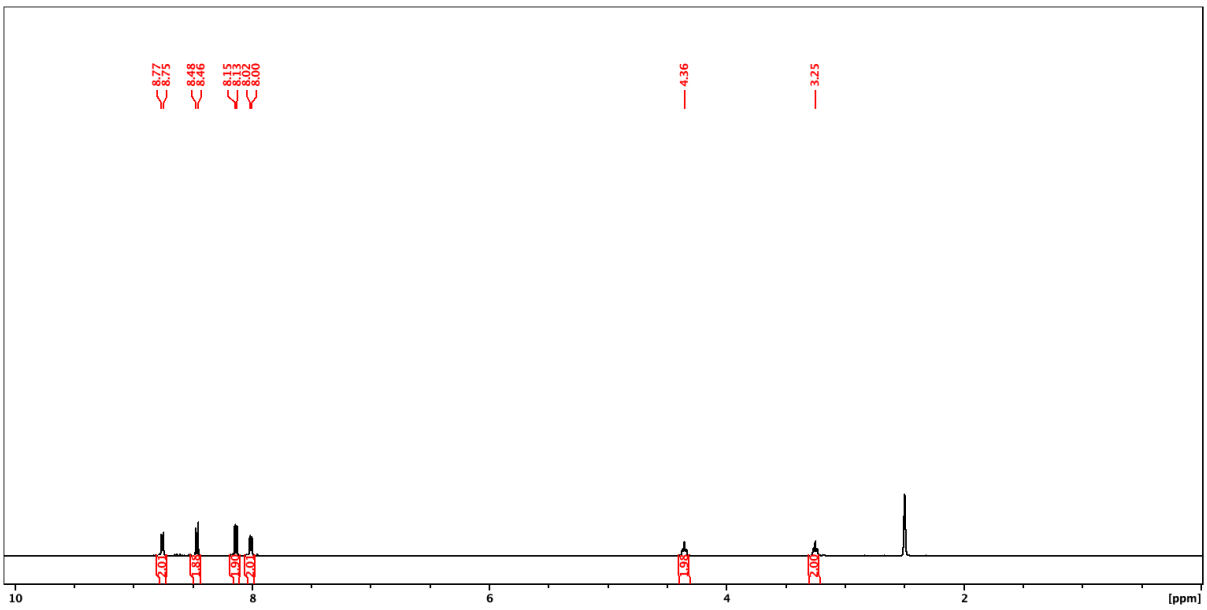
8.77
8.75
8.48
8.46
8.15
8.13
8.02
8.00
4.36
3.25
2.01
1.86
4.36
2.01
1.95
2.05
10
8
6
4
2
[ppm]

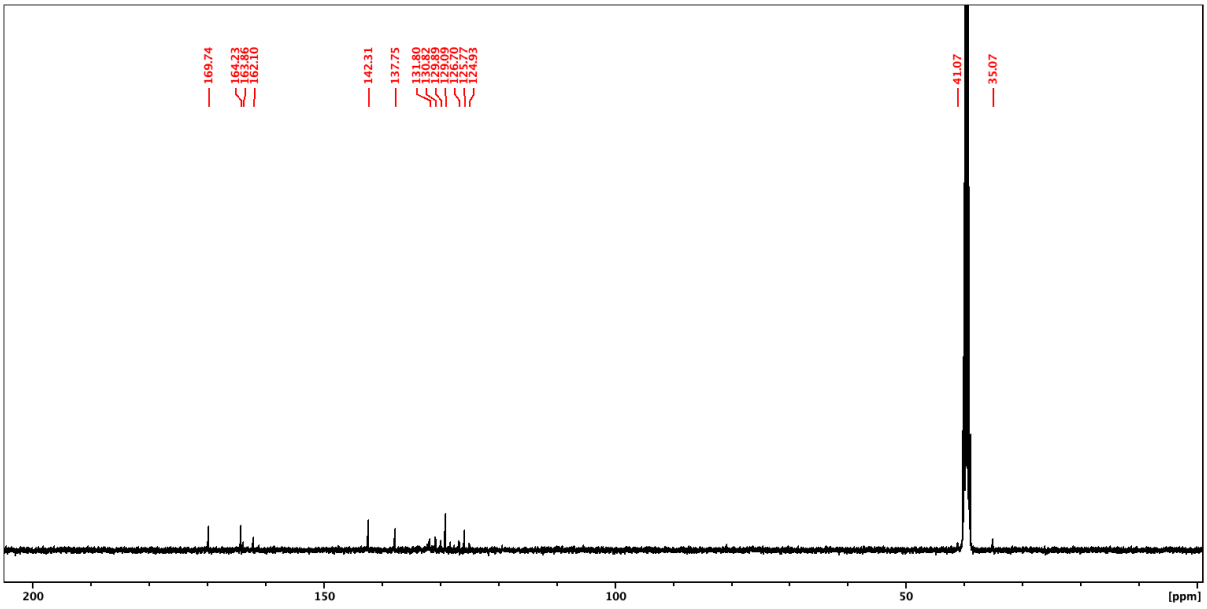
169.74
164.23
163.86
162.10
142.31
137.75
131.80
130.82
129.89
129.09
126.70
125.77
124.93
41.07
35.07
200
150
100
50
[ppm]

**NMI-2c**

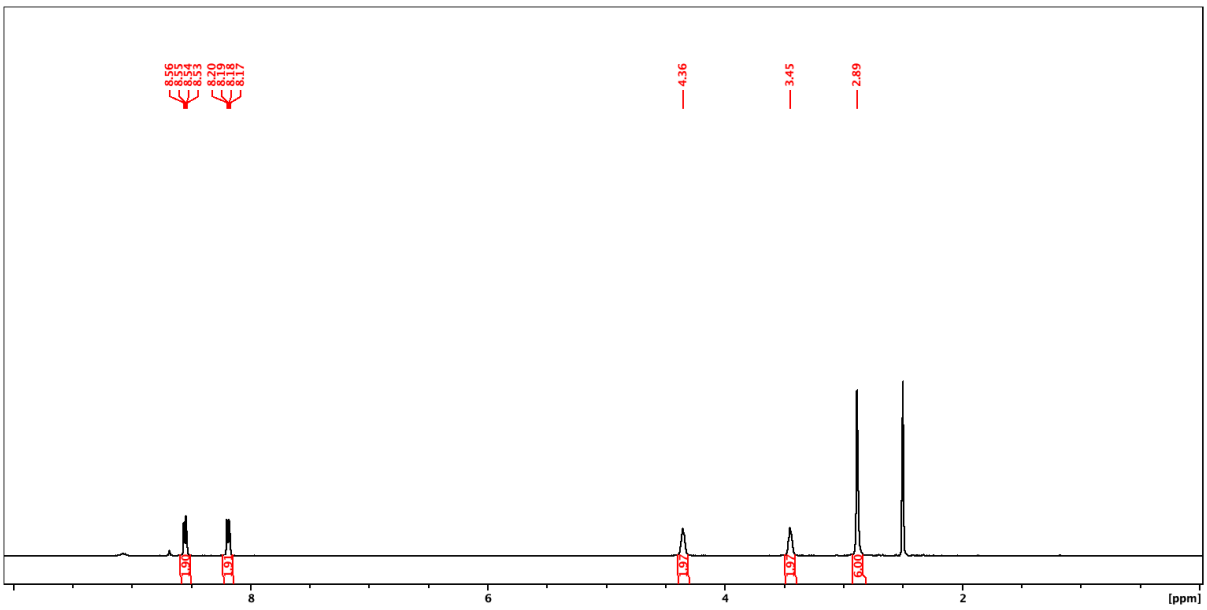
8.56
8.55
8.54
8.53
8.20
8.19
8.18
8.17
4.36
3.45
2.89
1.00
1.01
1.07
1.07
6.00
8
6
4
2
[ppm]

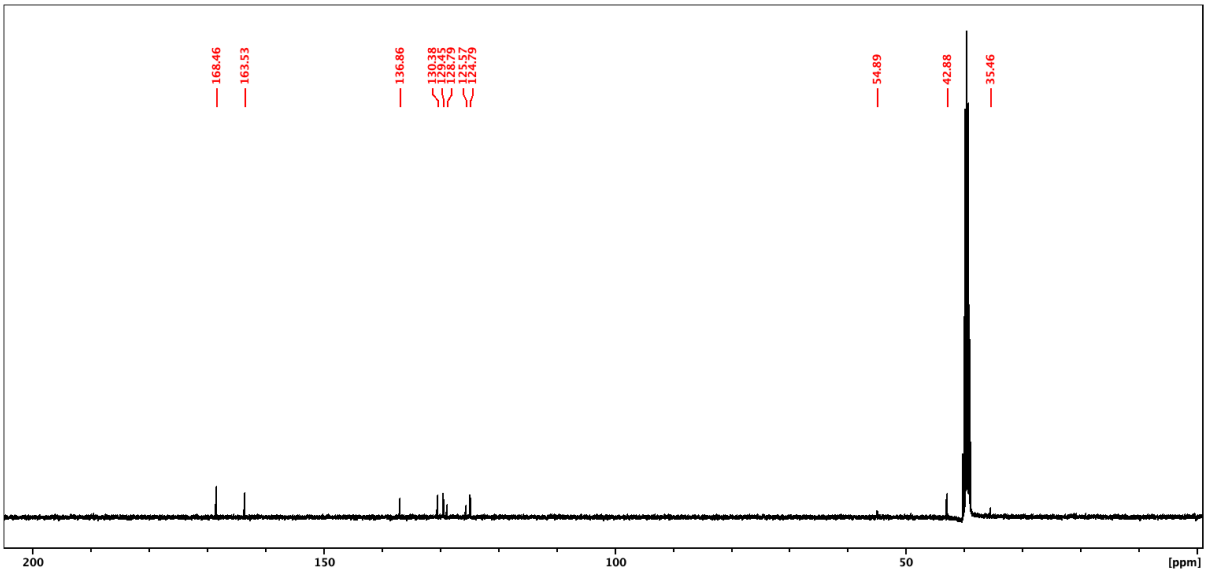
168.46
163.53
136.86
130.38
129.45
128.69
125.57
124.79
54.89
42.88
35.46
200
150
100
50
[ppm]

**NMI-2d**

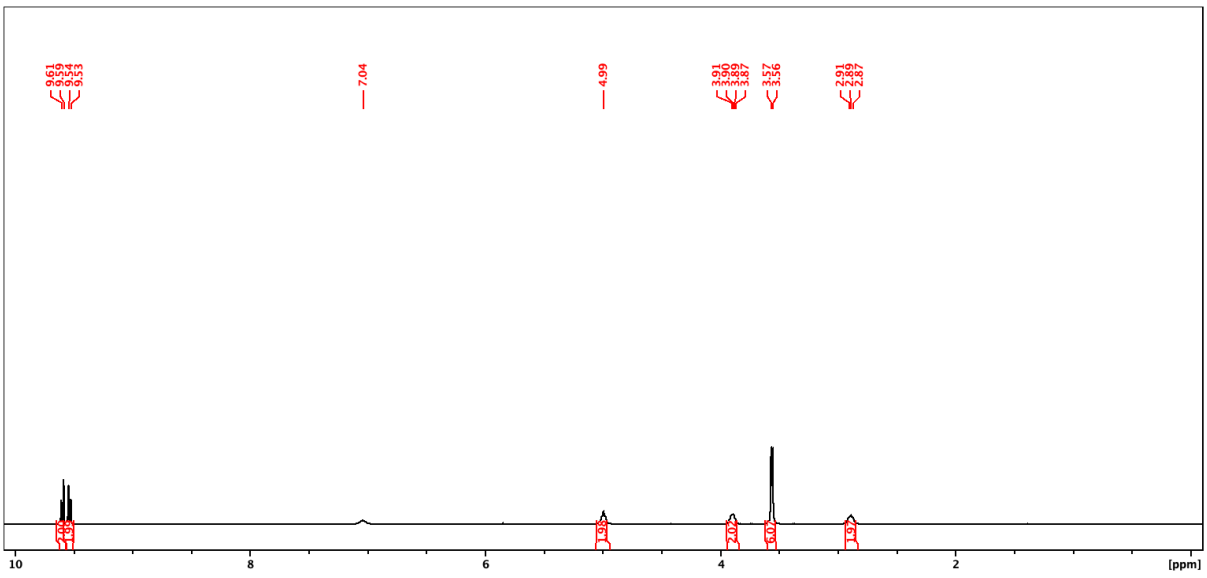
9.61
9.59
9.54
9.53
7.04
4.99
3.91
3.90
3.89
3.87
3.57
3.56
2.91
2.89
2.87
1.00
1.00
1.96
1.95
2.07
6.07
1.97
10
8
6
4
2
[ppm]

**NMI-3a**

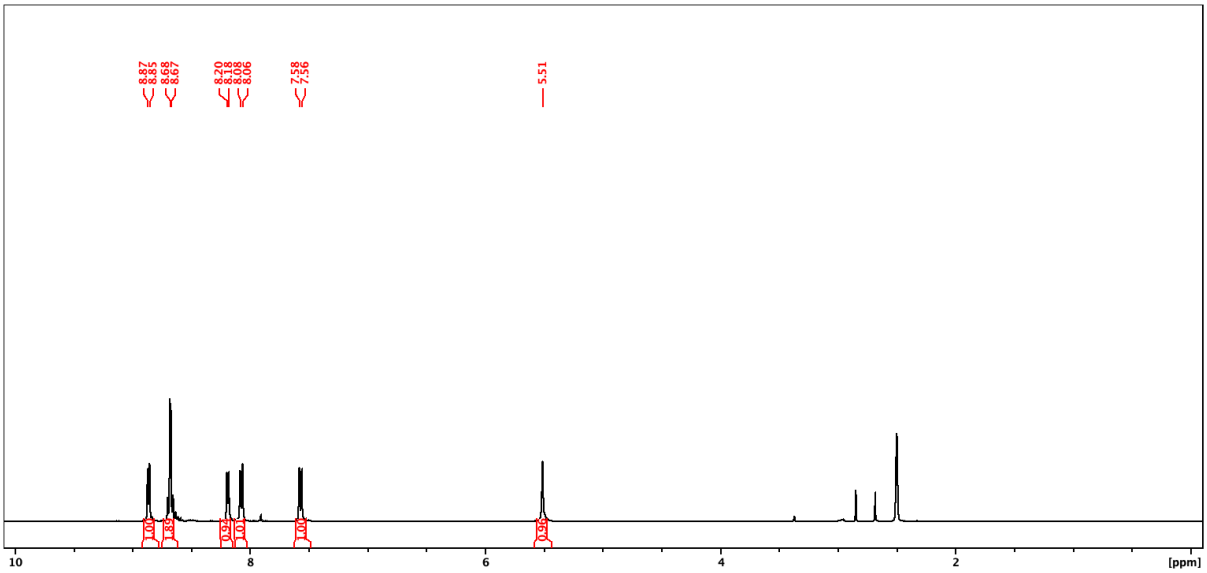
8.87
8.85
8.68
8.67
8.20
8.18
8.08
8.06
7.58
7.56
5.51
1.00
1.89
0.09
0.07
0.07
1.00
0.36
10
8
6
4
2
[ppm]

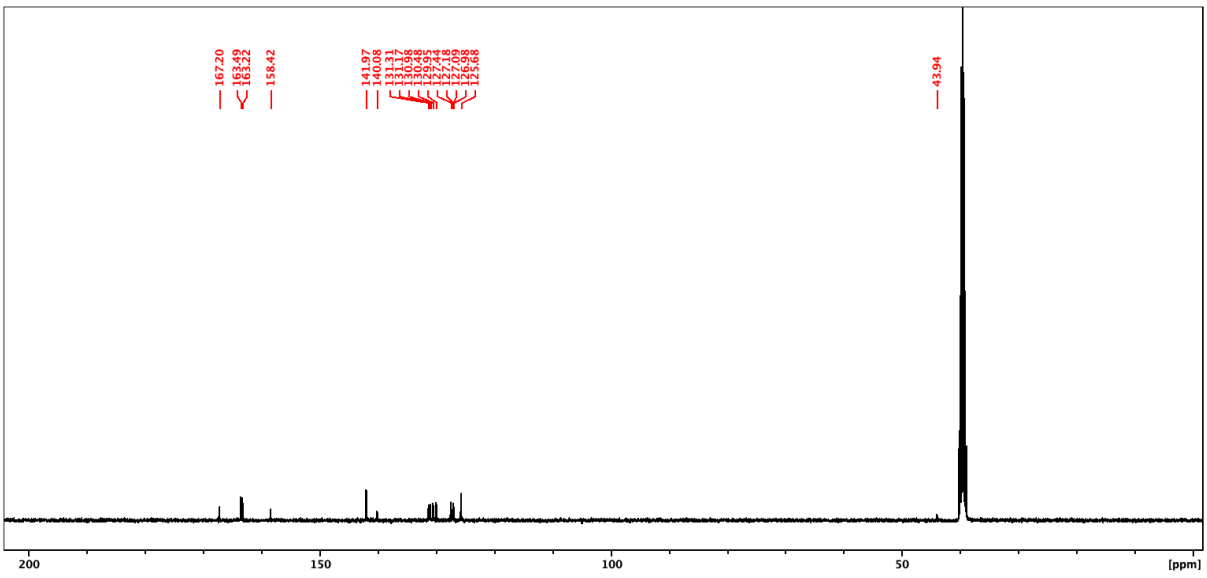
167.20
163.49
163.22
158.42
141.97
140.08
131.31
131.17
131.08
130.48
129.95
127.44
127.18
127.09
125.88
125.68
43.94
200
150
100
50
[ppm]

**NMI-3b**

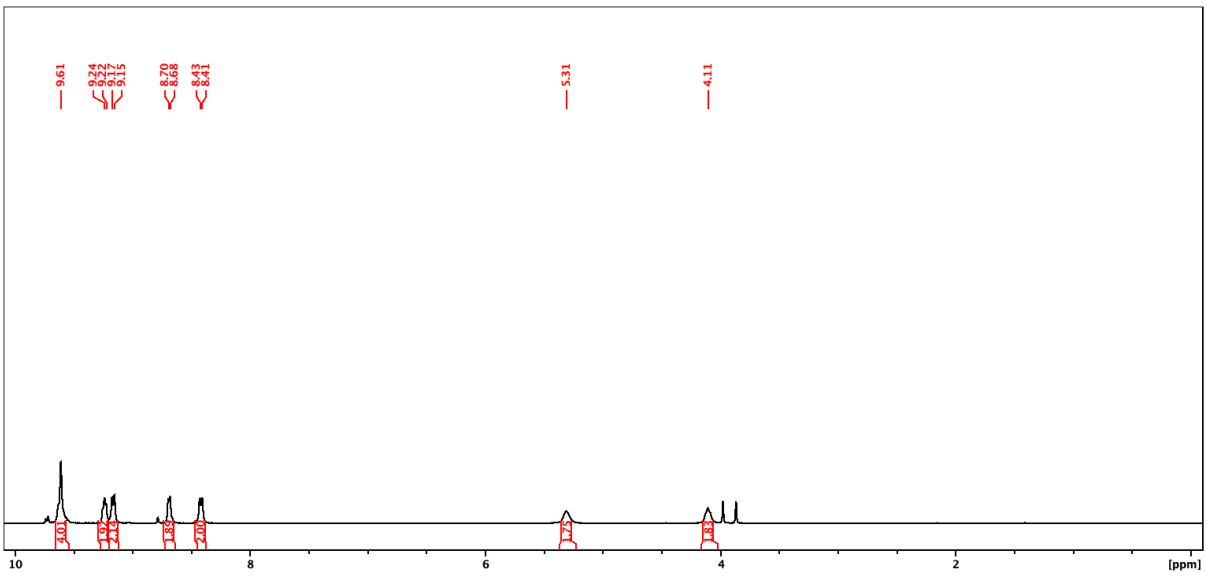
9.61
9.24
9.17
9.17
9.15
8.70
8.68
8.43
8.41
5.31
4.11
4.01
1.85
2.00
2.02
1.83
10
8
6
4
2
[ppm]

**NMI-3c**

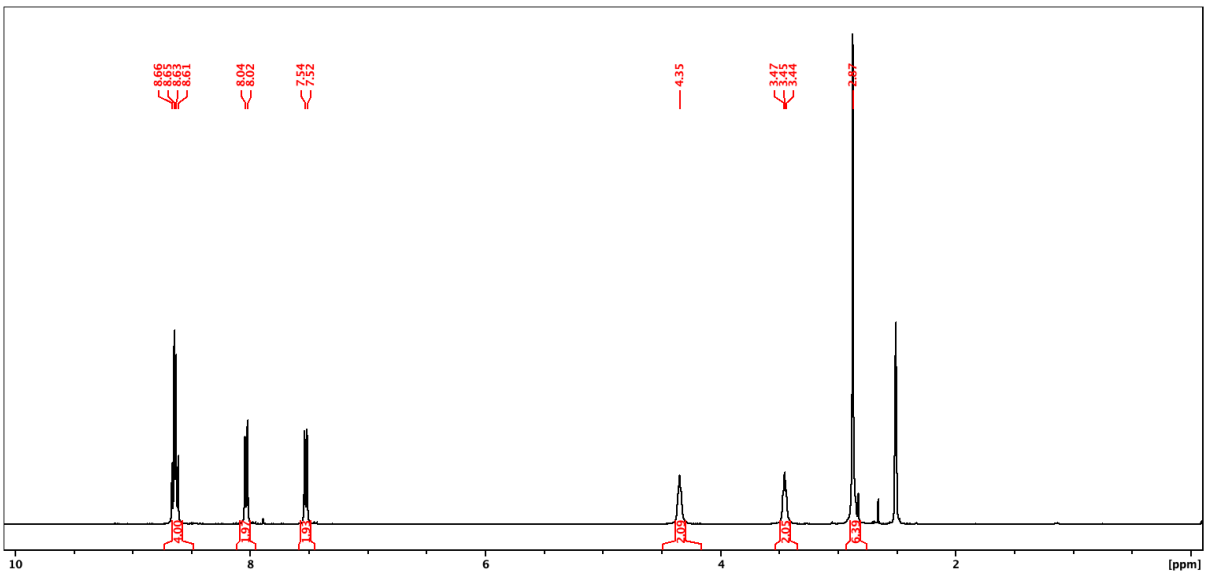
8.66
8.63
8.61
8.04
8.02
7.54
7.52
4.35
3.47
3.45
3.44
2.07
4.00
1.92
1.93
2.00
2.05
6.38
10
8
6
4
2
[ppm]

**NMI-3d**

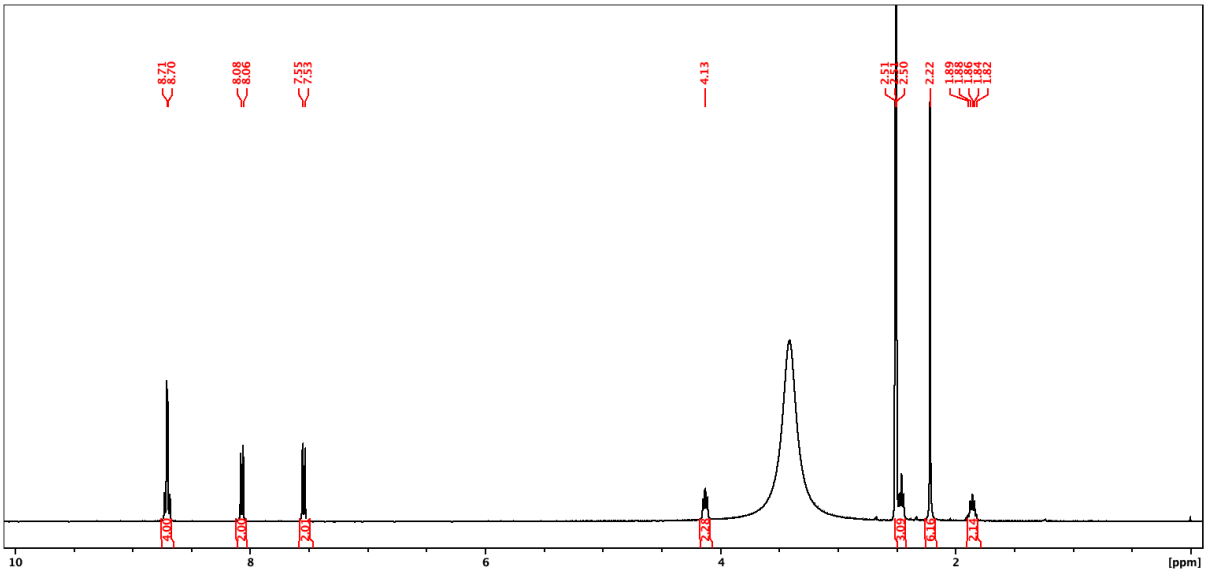
8.71
8.70
8.08
8.06
7.55
7.53
4.13
2.51
2.50
2.22
1.89
1.88
1.86
1.84
1.82
4.00
2.06
2.01
2.23
3.06
6.16
2.13
10
8
6
4
2
[ppm]

## 14. References


(1) Lu, J.; Lin, X.; Jiao, X.; Gengenbach, T.; Scully, A. D.; Jiang, L.; Tan, B.; Sun, J.; Li, B.; Pai, N.; et al. Interfacial Benzenethiol Modification Facilitates Charge Transfer and Improves Stability of Cm-Sized Metal Halide Perovskite Solar Cells with up to 20% Efficiency. *Energy Environ. Sci.* **2018**, *11* (7), 1880–1889. https://doi.org/10.1039/c8ee00754c.

(2) Yeh, J. J.; Lindau, I. Copyright 0 1985 by Academic Press, Inc. *At. Data Nucl. Data Tables* **1985**, *32* (l), 1–155.

(3) Rietwyk, K. J.; Wong, S. L.; Cao, L.; O'Donnell, K. M.; Ley, L.; Wee, A. T. S.; Pakes, C. I. Work Function and Electron Affinity of the Fluorine-Terminated (100) Diamond Surface. *Appl. Phys. Lett.* **2013**, *102* (9), 091604. https://doi.org/10.1063/1.4793999.

(4) Rietwyk, K. J.; Smets, Y.; Bashouti, M.; Christiansen, S. H.; Schenk, A.; Tadich, A.; Edmonds, M. T.; Ristein, J.; Ley, L.; Pakes, C. I. Charge Transfer Doping of Silicon. *Phys. Rev. Lett.* **2014**, *112* (15), 1–5. https://doi.org/10.1103/PhysRevLett.112.155502.

(5) Dontschuk, N.; Stacey, A.; Tadich, A.; Rietwyk, K. J.; Schenk, A.; Edmonds, M. T.; Shimoni, O.; Pakes, C. I.; Prawer, S.; Cervenka, J. A Graphene Field-Effect Transistor as a Molecule-Specific Probe of DNA Nucleobases. *Nat. Commun.* **2015**, *6* (1), 6563. https://doi.org/10.1038/ncomms7563.

(6) Jablonski, A.; Powell, C. J. Effective Attenuation Lengths for Different Quantitative Applications of X-Ray Photoelectron Spectroscopy. *J. Phys. Chem. Ref. Data* **2020**, *49* (3). https://doi.org/10.1063/5.0008576.

(7) Edmonds, M. T.; Wanke, M.; Tadich, A.; Vulling, H. M.; Rietwyk, K. J.; Sharp, P. L.; Stark, C. B.; Smets, Y.; Schenk, A.; Wu, Q.-H.; et al. Surface Transfer Doping of

Hydrogen-Terminated Diamond by C 60 F 48 : Energy Level Scheme and Doping Efficiency. *J. Chem. Phys.* **2012**, *136* (12), 124701. https://doi.org/10.1063/1.3695643.

(8) Schulz, P.; Schäfer, T.; Zangmeister, C. D.; Effertz, C.; Meyer, D.; Mokros, D.; Van Zee, R. D.; Mazzarello, R.; Wuttig, M. A New Route to Low Resistance Contacts for Performance-Enhanced Organic Electronic Devices. *Adv. Mater. Interfaces* **2014**, *1* (5), 1–8. https://doi.org/10.1002/admi.201300130.

(9) Meyer, D.; Schäfer, T.; Schulz, P.; Jung, S.; Rittich, J.; Mokros, D.; Segger, I.; Maercks, F.; Effertz, C.; Mazzarello, R.; et al. Dithiocarbamate Self-Assembled Monolayers as Efficient Surface Modifiers for Low Work Function Noble Metals. *Langmuir* **2016**, *32* (35), 8812–8817. https://doi.org/10.1021/acs.langmuir.6b01578.

(10) Choi, S. K.; Lee, J. I. Effect of Film Density on Electrical Properties of Indium Tin Oxide Films Deposited by Dc Magnetron Reactive Sputtering. *J. Vac. Sci. Technol. A Vacuum, Surfaces, Film.* **2001**, *19* (5), 2043–2047. https://doi.org/10.1116/1.1371326.

(11) López, G. P.; Castner, D. G.; Ratner, B. D. XPS O1s Binding Energies for Polymers Containing Hydroxyl, Ether, Ketone and Ester Groups. *Surf. Interface Anal.* **1991**, *17* (5), 267–272. https://doi.org/10.1002/sia.740170508.

(12) Meyer, D. Surface Functionalization with Amino-Based Self-Assembled Monolayers: Tailoring Electrode/Molecule Interfaces for Organic Electronics, Aachen University, 2015.

(13) Idriss, H. On the Wrong Assignment of the XPS O1s Signal at 531–532 EV Attributed to Oxygen Vacancies in Photo- and Electro-Catalysts for Water Splitting and Other Materials Applications. *Surf. Sci.* **2021**, *712* (April), 2–7. https://doi.org/10.1016/j.susc.2021.121894.

(14) Smets, Y.; Stark, C. B.; Schmitt, F.; Edmonds, M. T.; Lach, S.; Wright, C. A.; Langley, D. P.; Rietwyk, K. J.; Schenk, A.; Tadich, A.; et al. Doping Efficiency and Energy-Level Scheme in C60F48-Doped Zinc–Tetraphenylporphyrin Films. *Org. Electron.* **2013**, *14* (1), 169–174. https://doi.org/10.1016/j.orgel.2012.11.007.

(15) Frath, D.; Nguyen, V. Q.; Lafolet, F.; Martin, P.; Lacroix, J. C. Electrografted Monolayer Based on a Naphthalene Diimide-Ruthenium Terpyridine Complex Dyad: Efficient Creation of Large-Area Molecular Junctions with High Current Densities. *Chem. Commun.* **2017**, *53* (80), 10997–11000. https://doi.org/10.1039/c7cc04972b.

(16) Schenk, A. K.; Rietwyk, K. J.; Tadich, A.; Stacey, A.; Ley, L.; Pakes, C. I. High Resolution Core Level Spectroscopy of Hydrogen-Terminated (1 0 0) Diamond. *J. Phys. Condens. Matter* **2016**, *28* (30), 305001. https://doi.org/10.1088/0953-8984/28/30/305001.

(17) Chastain, J.; King, R. C. *Handbook of X-Ray Photoelectron Spectroscopy*; Perkin-Elmer, 1992.

(18) Wang, C.; Wang, H.-I.; Tang, W.-T.; Luo, C.-W.; Kobayashi, T.; Leu, J. Superior Local Conductivity in Self-Organized Nanodots on Indium-Tin-Oxide Films Induced by Femtosecond Laser Pulses. *Opt. Express* **2011**, *19* (24), 24286. https://doi.org/10.1364/oe.19.024286.

(19) Detweiler, Z. M.; Wulfsberg, S. M.; Frith, M. G.; Bocarsly, A. B.; Bernasek, S. L. The Oxidation and Surface Speciation of Indium and Indium Oxides Exposed to Atmospheric Oxidants. *Surf. Sci.* **2016**, *648*, 188–195. https://doi.org/10.1016/j.susc.2015.10.026.

(20) Donley, C.; Dunphy, D.; Paine, D.; Carter, C.; Nebesny, K.; Lee, P.; Alloway, D.; Armstrong, N. R. Characterization of Indium-Tin Oxide Interfaces Using X-Ray

Photoelectron Spectroscopy and Redox Processes of a Chemisorbed Probe Molecule: Effect of Surface Pretreatment Conditions. *Langmuir* **2002**, *18* (2), 450–457. https://doi.org/10.1021/la011101t.

(21) Fürer, S. O.; Milhuisen, R. A.; Kashif, M. K.; Raga, S. R.; Acharya, S. S.; Forsyth, C.; Liu, M.; Frazer, L.; Duffy, N. W.; Ohlin, C. A.; et al. The Performance-Determining Role of Lewis Bases in Dye-Sensitized Solar Cells Employing Copper-Bisphenanthroline Redox Mediators. *Adv. Energy Mater.* **2020**, 2002067. https://doi.org/10.1002/aenm.202002067.

(22) Surmiak, M. A.; Zhang, T.; Lu, J.; Rietwyk, K. J.; Raga, S. R.; McMeekin, D. P.; Bach, U. High-Throughput Characterization of Perovskite Solar Cells for Rapid Combinatorial Screening. *Sol. RRL* **2020**, *4* (7), 1–9. https://doi.org/10.1002/solr.202000097.

(23) Wang, J.; Fu, W.; Jariwala, S.; Sinha, I.; Jen, A. K. Y.; Ginger, D. S. Reducing Surface Recombination Velocities at the Electrical Contacts Will Improve Perovskite Photovoltaics. *ACS Energy Lett.* **2019**, *4* (1), 222–227. https://doi.org/10.1021/acsenergylett.8b02058.

(24) Diekmann, J.; Caprioglio, P.; Futscher, M. H.; Le Corre, V. M.; Reichert, S.; Jaiser, F.; Arvind, M.; Toro, L. P.; Gutierrez-Partida, E.; Peña-Camargo, F.; et al. Pathways toward 30% Efficient Single-Junction Perovskite Solar Cells and the Role of Mobile Ions. *Sol. RRL* **2021**, *5* (8). https://doi.org/10.1002/solr.202100219.

(25) Caprioglio, P.; Wolff, C. M.; Sandberg, O. J.; Armin, A.; Rech, B.; Albrecht, S.; Neher, D.; Stolterfoht, M. On the Origin of the Ideality Factor in Perovskite Solar Cells. *Adv. Energy Mater.* **2020**, *10* (27), 1–9. https://doi.org/10.1002/aenm.202000502.

(26) Calado, P.; Burkitt, D.; Yao, J.; Troughton, J.; Watson, T. M.; Carnie, M. J.; Telford, A. M.; O'Regan, B. C.; Nelson, J.; Barnes, P. R. F. Identifying Dominant Recombination

Mechanisms in Perovskite Solar Cells by Measuring the Transient Ideality Factor. *Phys. Rev. Appl.* **2019**, *11* (4), 1. https://doi.org/10.1103/PhysRevApplied.11.044005.